Copy number variation contributes to parallel local adaptation in an invasive plant

Jonathan Wilson[1], Paul Battlay[1], Vanessa C. Bieker[2], Lotte van Boheemen[1], Tim Connallon[1], Michael D. Martin[2], Kathryn A. Hodgins[1]

[1] School of Biological Sciences, Monash University, Melbourne, Victoria, Australia

[2] Department of Natural History, NTNU University Museum, Norwegian University of Science and Technology (NTNU), Trondheim, Norway

Abstract

Adaptation is a critical determinant of the diversification, persistence, and geographic range limits of species. Yet the genetic basis of adaptation is often unclear and potentially underpinned by a wide range of mutational types – from single nucleotide changes to large-scale alterations of chromosome structure. Copy number variation (CNV) is thought to be an important source of adaptive genetic variation, as indicated by decades of candidate gene studies that point to CNVs underlying rapid adaptation to strong selective pressures. Nevertheless, population genomic studies of CNVs face unique logistical challenges not encountered by other forms of genetic variation. Consequently, few studies have systematically investigated the contributions of CNVs to adaptation at a genome-wide scale. We present a genome-wide analysis of CNV contributions to the adaptation of an invasive weed, *Ambrosia artemisiifolia*, across its native and invasive ranges in North America and Europe, respectively. CNVs show clear signatures of parallel local adaptation between native and invasive ranges, implying widespread reuse of CNVs during adaptation to shared geographic patterns of selection. Using a local principal component analysis to genotype CNV regions in historic samples that span the last two centuries, we identified 16 large CNV regions of up to 11.85 megabases in length, six of which show signals of rapid evolutionary change, with pronounced frequency shifts between historic and modern populations. Our results provide compelling genome-wide evidence that copy number variation underlies rapid adaptation over contemporary timescales of natural populations.

Significance Statement

Using a population genomic approach, we identified copy number variation (CNVs) displaying parallel signatures of local adaptation across the native and introduced ranges of the invasive weed *Ambrosia artemisiifolia*. We further identified 16 large CNVs associated with ecologically important traits, including sex allocation and height, that show strong signatures of selection over space and time, along with dramatic temporal changes over the past several decades. These results highlight the importance of copy number variation in both local adaptation and rapid adaptation of invasive species.

Introduction

Understanding how populations adapt and persist in the face of rapid environmental change is one of the most pressing challenges of our time. Fundamental to this goal is determining the genetic basis of adaptive evolution. But despite considerable empirical and theoretical work in this area, many questions remain unresolved. For example, does adaptation typically rely on new, beneficial mutations or on standing genetic variation? Does adaptation generally result in the removal or maintenance of genetic variation affecting fitness? Do mutations contributing to adaptation have uniformly small phenotypic effects, or are large-effect mutations important as well? Do populations exposed to similar environments evolve using the same or different genetic variants?

The evolution of quantitative traits was traditionally thought to almost exclusively depend on evolutionary changes at many polymorphic loci with individually small phenotypic effects (1, 2). However, comparatively recent theoretical and empirical studies demonstrate that large-effect variants can also play important roles in adaptation (3-5). Large-effect mutations are particularly likely to contribute to the initial stages of a population's evolutionary response to a sudden shift in the environment (6), and to stable adaptive genetic differentiation among populations connected by migration. Such large-effect variants contribute to local adaptation by resisting the swamping effects of gene flow (7), including cases in which the alleles carry substantial pleiotropic costs (8).

Genomic structural variants, which include inversions, translocations, duplications and deletions, are predicted to have both large phenotypic effects and strong potential to contribute to adaptation (9, 10). Chromosomal inversions have a long history of evolutionary study, initially facilitated by classical cytogenetics (e.g., polytene chromosome studies [11, 12]), and more recently through advances in genome sequencing and analysis, which has produced compelling new evidence that inversions often underpin adaptation to environmental change (13–15). These findings have reinvigorated interest in the role of inversions in adaptation, yet other types of structural variation have not garnered the same level of attention.

Several case studies show that copy number variants (CNVs) – structural changes that include gene duplications, deletions and variation in transposable element abundance – have facilitated adaptation in well-characterized systems such as *Drosophila melanogaster* (16),

Anopheles gambiae (17), and *Arabidopsis thaliana* (18). Prominent examples include the repeated contribution of CNVs to pesticide resistance (19–22), evident in the parallel evolution of CNVs as a response of the agricultural weed *Amaranthus tuberculatus* to glyphosate exposure (23), and amplification of cytochrome P450 family genes in Antarctic killifish and fall armyworm populations exposed to toxins (24, 25). These studies demonstrate the immense adaptive potential of CNVs, yet most are candidate-driven analyses that cannot resolve the broader contributions of CNVs to adaptation. Few studies have systematically characterized the genome-wide contributions of CNVs to adaptive divergence across a range of environmental conditions and stresses (13, 26, 27).

Invasive species have several unique features that make them powerful systems for studying adaptation in nature, along with its genetic basis. First, because recently introduced populations are likely to be initially maladapted to local conditions in the new range, there is strong scope for rapid adaptive evolution that is observable within decades (28, 29). Second, some plant invasions have extensive documentation in geo-referenced herbarium collections that can be phenotyped and sequenced to identify and track evolutionary changes over time – an achievement that is rarely possible in natural populations (15, 30, 31). Third, invasive species typically occupy climatically diverse native and invasive ranges, promoting adaptive evolution to local environmental conditions (28, 29, 32). Their broad range breadths further enable tests of the predictability of evolution, since local adaptation across native and invasive ranges may stem from parallel or unique genetic solutions to similar environmental challenges (15, 32, 33). Despite these features making invasive species valuable for studying the genetic basis of adaptation, they remain underutilized. Moreover, they are also well suited for evaluating contributions of CNVs, which have been predicted to be important in invasive species adaptation (34, 35), though few studies have tested this hypothesis.

Over the last 200 years, the North American native plant *Ambrosia artemisiifolia* (common ragweed) has become a widespread pest in all continents except Antarctica (36). This wind-pollinated, outcrossing species produces highly allergenic pollen that accounts for ~50% of hay-fever cases in Europe (37). It is also an agricultural pest (38), with glyphosate resistance – a phenotype associated with CNVs in other species (19) – reported in some *A. artemisiifolia* populations (39). Previous studies show that *A. artemisiifolia* has established strong signals of local adaptation to climate across its native range, and in introduced ranges in Europe, Asia, and Australia, with rapid local adaptation following each introduction (15, 33, 40–44).

We have previously demonstrated a significant contribution of chromosomal inversions to climate adaptation in Europe and North America (15), which raises the question of whether CNVs have similarly contributed to adaptive divergence following *A. artemisiifolia's* range expansion.

In this study, we investigated the genome-wide contribution of CNVs to local adaptation in *A. artemisiifolia*. Our dataset, which includes over 600 whole-genome sequences from individuals collected across the native North American range and the introduced European range, including herbarium samples dating back to 1830, provided a unique opportunity to detect signals of adaptation over space and time. We first investigated whether putative CNVs display signatures of divergent selection in both Europe and North America. By comparing the selection signatures of putative CNVs in each range, we then assessed the degree to which these variants evolve in parallel between them. Second, using a subset of 121 phenotyped individuals, we tested for associations between putative CNVs and ecologically important traits, such as flowering time and size. We then developed a novel approach that combines read-depth and local PCA methods to genotype large CNV regions in both modern and low-coverage historic samples, which enabled us to estimate temporal changes in CNV frequency and thus directly track CNV evolution in these populations.

Results

CNV identification

To identify CNVs, we used read-depth for non-overlapping 10 kbp windows (normalized by the average coverage of each individual sample) in 311 modern re-sequenced genomes spanning both the North American and European ranges of *A. artemisiifolia*. We defined a window as a CNV if at least 5% of samples had average standardized read-depths either greater, or less, than two standard deviations from the window mean across samples. Out of the total 105,175 genomic windows, this resulted in 17,855 candidate CNVs retained for subsequent analyses.

CNV selection analysis

Local adaptation to spatially heterogeneous environments is expected to leave a signal of extreme allele frequency differentiation among populations (45). As our measures of read-depth for candidate CNV windows are continuous, we used a Q_{ST}-F_{ST} outlier test to identify windows with population differentiation in excess of neutral expectations. We first calculated

an F_{ST} distribution of neutral SNPs (Figure 1B, D), using the method of Weir & Cockerham (46). Under neutrality, F_{ST} and Q_{ST} values should have similar distributions, whereas an enrichment of Q_{ST} values within the tails of this null F_{ST} distribution provides evidence for local adaptation, with Q_{ST} outliers representing local adaptation candidates (47).

In North America, 1,382 CNV windows exhibited Q_{ST} values at or above the top 1% of neutral F_{ST} values, which is a 7.7-fold enrichment relative to the neutral expectation that 1% of Q_{ST} windows will fall within this tail ($p < 2.2e-16$; binomial test; Figure 1A, B). In Europe, 339 CNV windows exhibited Q_{ST} values exceeding the top 1% of the F_{ST} distribution, a 1.9-fold enrichment (Figure 1C, D; $p < 2.2e-16$; binomial test). This excess of outliers is consistent with a true positive rate of 87% for the North American CNV candidate windows, and 47% true positives for European outlier windows. Of the CNV windows displaying differentiation, 111 were outliers in both ranges (32% of European outliers; p=1.17e-40, hypergeometric test; Figure 2A), which is a highly significant excess indicative of parallelism in the same CNVs subject to divergent selection in both ranges.

To identify candidate CNVs associated with climate, we estimated correlations between each candidate CNV window and six bioclimatic variables (Supplementary Figure 4; 5), after filtering highly-correlated variables from the original 19 WorldClim variables (48). Of the 1,382 significant Q_{ST} windows in North America, 315 (22.7%) were associated with at least one of the seven climate variables, whereas only 12 of 339 significant windows in Europe (3%) correlated with climate variables (Supplementary Figures 4; 5). This suggests that the primary selective forces driving differentiation of CNVs in Europe are likely not climate related.

To determine the putative biological functions of the adaptation candidates we used gene ontology (GO) enrichment analyses of annotated genes residing within the outlier Q_{ST} windows. We found that candidate CNVs in North America are enriched for biotic and abiotic stress response genes, with significant GO terms including “systemic acquired resistance,” “response to oomycetes”, and “response to freezing” (Supplementary Figure 2A; Supplementary Table 1). In Europe, significant GO enrichments included the hormonal stress response pathways “response to abscisic acid” and “response to jasmonic acid” (Supplementary Figure 2B; Supplementary Table 2). The overlapping Q_{ST} candidates

between the ranges exhibited GO term enrichment for the defense response terms “defense response to virus” and “response to abscisic acid” (Figure 2B; Supplementary Table 3).

CNV-trait associations

We tested for relationships between genome-wide CNVs and 29 ecologically important traits that were phenotyped in 121 of our samples, each reared in a common garden experiment (phenotype data were previously reported in van Boheemen, Atwater & Hodgins [41]). Eighteen traits (Supplementary Table 5) were significantly associated with normalized read-depth in at least one of our 17,855 candidate CNV windows (Supplementary Figure 3). Of particular interest, two nearby windows on chromosome 14 (h1s14:17180001-17190000, h1s14:18470001-18480000) were associated with flowering onset, dichogamy, and sex allocation (defined as female reproductive biomass/male reproductive biomass) (Supplementary Figure 3). These traits display strong latitudinal clines in *A. artemisiifolia*, with overall earlier flowering, much earlier male flowering than female flowering, and female-biased sex allocation occurring at high absolute latitudes (41). These two windows flank an annotated gene, AGL-104, that is linked to pollen production in *Arabidopsis* (49). Moreover, one of these windows (h1s14:18470001-18480000) is a Q_{ST} outlier in North America and Europe, indicating parallel divergent selection.

Large CNV region identification (CNVr)

The continuous measures of read-depth in 10 kbp windows appeared to give unreliable results with the low-coverage historic data. Since we had previously obtained accurate measures of genotypes for large inversions in these historic samples (15), we implemented a similar approach to identify large CNV regions (CNVr) in order to perform temporal comparisons. Furthermore, many CNVs could be larger than 10 kbp. We therefore used a linkage disequilibrium based approach to merge adjacent windows with highly correlated read-depth ($R^2 > 0.6$), which indicates that they are components of a larger CNV. After merging windows, the number of candidate CNVs was reduced from 17,855 to 11,877, with the largest window measuring 11.85 Mbp on chromosome 4. To corroborate the presence of large segregating CNVs within our dataset, we performed a local PCA of genotype likelihoods in 100 kbp windows across the genome. We determined potential segregating structural variants as regions with at least three adjacent windows that were outliers for distortions in local population structure relative to the rest of that chromosome. This resulted in a minimal size cutoff for CNVrs of 300 kbp. As such, we defined CNV regions as those in which merged read-depth windows greater than 300 kbp overlapped with windows exhibiting

variation in local population structure. Using this approach we identified 52 candidate CNVrs.

We then genotyped individuals for CNVrs in our population genomic data, including low coverage historic samples. To do this, we used a combination of normalized read-depth for each candidate CNV region alongside a PCA calculated within that same region to cluster samples into genotypes which differed in both read-depth and PC1 (Figure 3). With this approach, we were able to identify distinct clusters corresponding to genotypes in 16 out of 52 CNVrs. These 16 CNVrs accounted for 8.1% of the 17,885 10 kbp windows, including 22.6% of outlier Q_{ST} windows in North America and 7.2% of outlier Q_{ST} windows in Europe. These large CNVrs ranged in size from 0.3 - 11.85 Mbp. Fifteen of these CNVrs exist as heterozygotes within the diploid reference genome, with haplotype 1 containing presence variants, meaning they can be corroborated with alignments between each haplotype of the diploid assembly (Supplementary Figure 8). The high heterozygosity within the reference was likely caused by the fact that our genotyping method favored loci where the absence allele was common in our sample, yet the presence alleles needed to be found within the haplotype 1, which acted as our reference, in order for the CNV to be identified. This is consistent with the low frequencies (mean = 0.196; range: 0.027 -0.479) of all CNVr presence variants (Supplementary Table 6). GO analysis of annotated genes indicates that the 16 CNVrs are enriched for several biological processes, including “methylglyoxal catabolism”, “peroxisome fission”, “pollen tube adhesion”, and “glyphosate metabolism” (Supplementary Table 4).

Of particular interest is the massive cnv-chr4a region, which is 11.85 Mbp in length by our estimation method. Closer inspection of this region within the diploid reference reveals that large regions on haplotype 1 are absent on haplotype 2, but are interspersed by 3 smaller inversions (Figure 3; Supplementary Figure 7; 8). Analysis of coverage depth across chromosome 4 of three closely related Ambrosia species sequences mapped to the *A. artemisiifolia* reference revealed that the absence variant is likely ancestral (Supplementary Figure 9). The derived insertion variant contains an excess of transposable elements (TEs) relative to the remainder of chromosome 4 (87.21% versus 70.48%). TE family Ty1/Copia accounts for 32.45% of the TEs within cnv-chr4a, compared to just 14.87% throughout the rest of this chromosome. Repetitive elements display greater density towards the beginning of this region (Supplementary Figure 10), which corresponds to regions of lower gene density.

The greater gene density toward the end of the cnv-chr4a region shows strong synteny with chromosome 2 and aligns with inversions present in the reference alignment (Supplementary Figure 7; 10). Most of chromosome 4 displays synteny with chromosome 2, suggesting they are homoeologous chromosomes. The largest gap in syntenic blocks corresponds to the gene-depleted and TY1/Copia-enriched region of cnv-chr4a (Supplementary Figure 10). It is therefore likely that this complex structural variant consists of a series of inversions which have subsequently been separated by a large TE expansion. Recombination is likely strongly suppressed within this region, as the coverage windows exhibit strong linkage disequilibrium across the region. The candidate CNV windows within cnv-chr4a are Q_{ST} outliers (Figure 1A; C) and associated with the bioclimatic variable mean diurnal range (Supplementary Figure 4), consistent with contribution to local adaptation.

Another noteworthy CNVr on chromosome 8, cnv-chr8a, contains an ortholog of the *Arabidopsis thaliana* EPSPS locus. This CNVr lies within a large inversion, hb-chr8, previously described in Battlay et al. (15). The frequency of cnv-chr8a is not correlated with the frequency of this inversion, yet cnv-chr8a presence alleles occur exclusively on the common, and presumably ancestral, orientation of the inverted region.

Spatio-temporal CNVr modeling

We used whole genome sequences derived from >300 historical herbarium samples (dating back to 1830) and generalized linear models (GLMs) to understand how the 16 CNVr alleles may have changed in frequency over both space and time. These GLMs predicted genotype as a function of range (native or introduced), latitude and year of collection, and were reduced to contain any significant interactions between these variables. To correct for population structure, we also included PC1 from a PCA calculated on 10,000 neutral SNPs as a covariate in each model. Twelve of the 16 CNVrs displayed at least one significant predictor variable (time, range, latitude or interactions). Nine CNVrs exhibited significant associations with latitude (cnv-chr4a, cnv-chr4b, cnv-chr5a, cnv-chr9a, cnv-chr14a, cnv-chr17b, cnv-chr17c and cnv-chr18a) (Supplementary Table 7; Supplementary Figure 11). Models of three CNVrs (cnv-chr10a, cnv-chr14a and cnv-chr17a) contained significant three-way interactions (Figure 4; Supplementary Table 7; 8; Supplementary Figure 11). Of note, both cnv-chr14a and cnv-chr17a displayed clinal patterns in North America regardless of year, whereas this same latitudinal pattern was present only in modern European samples—strong evidence of clinal reformation an initial period of maladaptation in the introduced

range (Figure 4; Supplementary Table 7; 8). The large insertion in cnv-chr4a displays latitudinal clines in modern populations across both ranges, with higher insertion frequencies at lower latitudes. In the native range, this appears to be driven by increasing frequencies over time in more central and southern populations of North America (Supplementary Table 8). This CNV overlaps with a previous SNP-based result consistent with a selective sweep in the St. Louis population (15).

To further analyze the potential adaptive significance of these CNVrs, we assessed associations between each variant and 29 phenotypes that were previously measured in a common garden experiment (41) in 123 contemporary samples included in this study. Cnv-chr10a displayed Bonferroni-significant associations with total biomass, root weight and total number of male inflorescences, whilst cnv-chr14a was significantly associated with sex allocation (Supplementary Table 9).

Discussion

CNVs are increasingly recognized as important in local adaptation (13, 24, 26, 27, 50). However, previous empirical evidence is predominantly limited to contexts of pesticide resistance (18, 25) and various candidate gene studies (51, 52). We implemented a genome-wide discovery approach to identify CNVs that might contribute to local adaptation and examined their potential contributions to local adaptation across the native and an invasive range of *A. artemisiifolia*. Our previous work provided strong evidence that several chromosomal inversions contribute to local adaptation across these ranges, and the current study supports an additionally important role for CNVs. CNV windows were enriched for signatures of local adaptation, much of it occurring in parallel between native and invasive ranges. Furthermore, large CNV regions identified in modern and historical samples show evidence of rapid local adaptation across the short timescale (ca. 150 years) of *A. artemisiifolia's* invasion in Europe.

Ambrosia artemisiifolia CNV windows exhibited extensive signals of local adaptation, including elevated geographic divergence in fold coverage, relative to neutral expectations, in both North America and Europe (Figure 1). These windows show an over-representation of genes involved in abiotic and biotic stress responses in North America (Supplementary Figure 2A, Supplementary Table 4) and pathogen defense in Europe (Supplementary Figure 2B, Supplementary Table 3) – consistent with F_{ST} outlier loci in Europe being enriched for

defense related functions (30). The overall weaker patterns of CNV differentiation in Europe relative to North America are consistent with previous SNP-based analyses showing fewer differentiated outlier SNP windows in Europe (15). Some CNVs were associated with traits important to local adaptation, including a window on chromosome 16 CNV associated with mature plant height (Supplementary Figure 3), which also overlaps an annotated NB-ARC domain. These domains, which occur within most plant resistance (R) genes, are involved in nucleotide binding and recognition (53), and duplications of such genes are known to underlie the evolution of resistance to various pathogens (54, 55). Our CNVs also appear to influence phenological traits. For example, the CNV windows on chromosome 14 are associated with flowering time (Supplementary Figure 3). Overall, our data point to important roles of CNVs in the local adaptation of *A. artemisiifolia*, which aligns with evidence from other species that structural variants widely contribute to adaptation (56–58).

One third of adaptive CNV windows in Europe were also candidates for adaptation in North America. Previous work in *A. artemisiifolia* has revealed similar patterns of repeatability, or parallelism, with respect to SNPs (15, 33), inversions (15), and genes affecting locally adapted traits like flowering time and sex allocation (41). Invasive species are expected to evolve in parallel when responding to analogous selection pressures, as in our system and others such as *Drosophila suzukii* and European starling (59, 60). Such parallelism is promoted when genetic variation involved in local adaptation in the native range is recruited as a source of adaptive variation within the invasive range (61, 62), and multiple introductions from several genetically diverse source populations from North America to Europe presumably facilitated repeatability by ensuring that most of the important variants successfully made the journey to the new range (30, 33). That all CNVrs were present in historical European populations indicates that they were introduced into Europe early on during the invasion (Supplementary Table 6).

The 16 large CNV regions that we detected using a combination of read-depth, linkage disequilibrium and local population structure analyses (Figure 3A, Figure 3B) contained 22.6% of Q_{ST} outlier windows from North America and 7.2% of the outlier windows from Europe. Yet these CNVrs comprised only 0.23% of the genome, demonstrating their disproportionate importance in local adaptation. Remarkably, 15 of the CNVrs co-localize with segregating deletions in the highly heterozygous diploid reference, supporting our detection method. Closer analysis of the largest CNVr (cnv-chr4a) within the reference

reveals that our detection method may lack sensitivity in fully revealing structural complexity within CNVrs (Figure 3). Multiple abutting inversions and CNVs within this region appear to segregate together as a single, complex structural variant. Nevertheless, the regions we identified demonstrate the general adaptive potential of structural variants, in which CNVs are predominant features. Since our method of detection for CNVrs was biased towards identifying large CNVrs with presence variants on haplotype 1 of the reference, and our genotyping method was biased towards identifying loci with common absence alleles, our results represent a lower bound on the prevalence and adaptive significance of CNVrs in *A. artemisiifolia*. Investigations using pangenomics (63) to elucidate a more complete picture of the contribution of CNVs to adaptation is therefore warranted.

Our study goes beyond the traditional population-genomic approach of detecting signals of local adaptation using contemporary samples alone. Our use of historical sequence data also allowed us to track temporal change in CNV frequencies across nearly two centuries—a period that spans the establishment and spread of *A. artemisiifolia* within Europe (36, 64), and significant environmental upheaval in both ranges, owing to industrialization, agriculture, and climate change (65). Eight CNVrs display clear frequency shifts over time, consistent with rapid adaptation over its recent evolutionary history. For example, while cnv-chr14a and cnv-chr17a both exhibit a consistent latitudinal cline in historical and modern North American populations, these clines are only evident in modern European populations (Figure 4A; Supplementary Table 7; 8), which is consistent with the rapid reformation of this cline in Europe following an initial period of maladaptation in this invasive range. This CNVr is associated with sex allocation (Supplementary Table 9), and candidate CNV-windows within the region exhibit associations with flowering time, sex allocation and dichogamy (Supplementary Figure 3). These traits show parallel clines in Europe and North America (41). Furthermore, this region lies within 20 kbp of the AGL-104 gene, which is involved in pollen development in *Arabidopsis* (49). Flowering time is a complex trait that is affected by numerous types of genetic variants (66). Our results indicate that SNPs, inversions (15), and CNVs each play important roles in the rapid adaptation of this important trait in *A. artemisiifolia* populations.

Many well characterized CNVs in other species are associated with the evolution of pesticide resistance (19, 20, 25). We identified a CNVr (cnv-chr8a) potentially involved in herbicide resistance. An ortholog of the *Arabidopsis thaliana EPSPS* locus, which lies within the cnv-

chr8a region, is the molecular target of glyphosate herbicides. CNVs confer resistance to glyphosate in numerous other weed species, where the increased gene expression caused by *EPSPS* gene amplification ameliorates the herbicide's toxic effects (19, 51). Glyphosate resistance has been documented in some *A. artemisiifolia* populations (39), and while we do not know which populations in our study might be glyphosate resistant, this CNVr is a strong candidate for future study.

Our study highlights the importance of copy number variation in the evolution of a broadly distributed and rapidly adapting invasive weed. While CNVs have previously been implicated in adaptation in response to specific selection pressures in other species (23, 24), our genome-wide discovery approach was able to identify candidate genomic regions that are more broadly representative of the broader contribution of CNVs to local adaptation. Several of these candidates strongly associate with specific traits, ranging from flowering time to pathogen resistance. Along with previous studies showing that SNPs and chromosomal inversions underlie local adaptation during *A. artemissifolia*'s expansion across vast environmental gradients, these new findings make it clear that CNVs account for a significant and previously unrecognized component of this plant's past success and are consequential for its invasive capacity wherever it may be introduced in the future.

Methods

Samples and alignments

Analyses were conducted on 617 whole-genome *Ambrosia artemisiifolia* sequences described in Bieker *et al*. (30) and a chromosome-level, phased, diploid *Ambrosia artemisiifolia* genome assembly (15). Alignments and SNP calls against the primary haplotype of the diploid reference (haplotype 1) were generated by Battlay *et al*., (15), using the Paleomix v1.2.13.4 (67) pipeline and GATK UnifiedGenotyper v3.7 (68). Modern and historic samples were sequenced from across the species' native North American (155 modern and 91 historic samples) and introduced European (156 modern and 192 historic samples) ranges. Modern samples were collected between 2014 and 2018 and historic samples were sequenced from herbarium samples collected between 1830 and 1973, with a median collection date of 1905 (Supplementary Figure 1). Present-day population samples, whose geographic coordinates were recorded during sampling, included between n = 2 to n = 10 individuals. Historic individuals were grouped into populations according to their proximity (15, 30). Cases where

only one sample was obtained from a geographic location were excluded from analyses in which population information was a requirement. Additionally, we aligned sequences of three other *Ambrosia* species (30) to the primary haplotype of the diploid reference using the Paleomix pipeline, as described in Battlay *et al.* (15).

Depth of coverage analysis

In order to identify copy number variation within our resequenced common ragweed individuals, we analyzed depth of coverage in non-overlapping 10 kbp windows using Samtools v1.9 *depth* (69) on alignment bam files. In the initial analyses of modern samples we only used reads with mapping quality > 30 (*-Q 30*). Subsequent read-depth analyses of historic samples used reads with mapping quality > 5 (*-Q 5*) in order to accommodate the poorer mapping quality of historic resequenced specimens. Each window was then normalized by dividing window depth by the genome-wide coverage for the sample. To apply a population frequency-based filter to this dataset, we kept only windows which had at least 5% of samples greater than or less than 2 standard deviations from the population mean. This filtering procedure resulted in 17,855 of 105,175 windows (5.8%) being classified as copy number variants (CNVs).

Q_{ST}-F_{ST} analysis

Genomic loci that have responded to spatially heterogeneous selection are expected to show elevated differentiation among populations, relative to neutrally evolving loci. SNPs associated with local adaptation can be detected as outliers of genome-wide scans of F_{ST} or similar statistics (46, 70, 71). However, unlike SNP data, candidate CNVs have been identified by depth of coverage, which is represented on a continuous scale. As such, coverage can be viewed as a phenotypic measurement that is analogous to measurements of continuous traits. Tests for trait responses to divergent selection are often inferred using a Q_{ST}-F_{ST} analysis (72, 73). Theory predicts that Q_{ST} values for neutrally evolving traits should follow the same distribution as F_{ST} for neutrally evolving loci (47). We used coverage data to measure Q_{ST} values for each window (analyses were conducted separately for the European and North American ranges), adapting the relationship between Q_{ST} and population variation from Whitlock (47):

$$Q_{ST} = V_{A,among} / (V_{A,among} + 2V_{A,within}) \quad (1)$$

where $V_{A,among}$ represents the among-population variation in coverage for a given window, and $V_{A,within}$ represents within-population coverage variation.

We performed linear mixed models, using the lme4 package (74) on populations from each range to extract variance components attributed to within- and among-population variation for each coverage window. Unlike other analyses performed in this study, we used unnormalised coverage for each window in the model, and accounted for variation in individual sample depth by including individual median coverage as a covariate in the model, and population was included as a random effect. The variance among populations ($V_{A,among}$) was extracted as the variance component attributed to the population, and within-population variance ($V_{A,within}$) corresponded to the model's residual variance component.

To identify Q_{ST} values with divergence in excess of neutral expectations, the distribution of Q_{ST} values in each range was compared to the distribution of neutral F_{ST} values from the same populations. F_{ST} distributions were calculated in VCFtools (75) using 10,000 putatively neutral and independently segregating LD-pruned SNPs, randomly sampled from outside both genic regions and known structural variants (15). Outliers were classified as windows with Q_{ST} values greater than 99% of neutral F_{ST} values. Under neutrality, 1% of Q_{ST} values are expected to fall above this 99% threshold, and we therefore tested whether there was a significant excess of windows above this null expectation. Analyses were performed using modern data from North America and European ranges separately.

Environmental-CNV Associations

Correlations between genetic variation and environment provide further evidence for local adaptation on the genomic level. CNV-environment associations were identified by measuring Spearman's correlation coefficients (Rho) between normalized coverage of each 10 kbp window and climate variables. Climatic variables were extracted from WorldClim (48) for each of the geographic coordinates of our sample of individuals. We excluded highly correlated variables ($R^2 > 0.7$) from the analysis, resulting in six variables: BIO1: annual mean temperature, BIO2: mean diurnal range, BIO8: mean temperature of wettest quarter, BIO9: mean temperature of driest quarter, BIO12: annual precipitation, and BIO15:

precipitation seasonality. Outliers were identified as the top 1% of the empirical p-value of the Rho distribution. Coverage windows that were in the 1% tails of the CNV-environment distribution and outliers in our Q_{ST} analysis were considered CNV-climate adaptation candidates.

Identifying large CNV regions

Since larger CNVs will affect coverage in multiple adjacent windows, we used a linkage disequilibrium-based approach to merge nearby windows. We merged windows within 1 Mbp (and all windows within this region) that had sample depths that were correlated at $R^2 > 0.6$. By generating heatmaps of LD between CNV windows, we visualized the presence of correlated read-depth, indicative of larger CNVs (Supplementary Figure 6). This resulted in 11,877 windows ranging in size from 10 kbp to 11.85 Mbp.

Local principal component analysis has previously been used to detect population-genomic signatures of chromosomal inversions (15, 56, 76). Here we employed this method to identify distortions in local relatedness due to CNVs using two modifications. Firstly, we calculated local covariance matrices for each window using ANGSD (77) and PCAngsd (78). Secondly, we did not include a filter for missing data in our ANGSD command, which meant that missingness would cause distortion in the local PCAs. The analysis was performed in non-overlapping windows of 100 kbp, and multidimensional scaling axes 1-4 (calculated from local PCAs across each chromosome) were examined for blocks of outliers indicative of large structural variants. While individual MDS outlier windows are not necessarily due to structural variations, SVs are the most likely cause of signals that are consistent across adjacent windows. Therefore, we retained candidates that included at least three adjacent windows that were outliers, so that the lower limit of CNVr size was 300 kbp. As such, we identified candidate CNVr as those where MDS candidates overlapped the merged read-depth-based CNV windows which were also greater than 300 kbp in length. These 52 candidate CNVrs corresponded to 68% of the merged CNV windows greater than 300 kbp in length.

CNV region genotyping

We attempted to genotype modern and historical samples, separately, for each of the 52 candidate CNVr. To do so, we performed another local PCA across the length of each candidate CNVr using PCAngsd (78). We then compared PC1 of the candidate CNVr against the average normalized read-depth across that CNVr to identify whether individuals clustered

along the lines of both read-depth and PC1. To genotype these samples according to these clusters, we used k-means clustering from the ClusterR package in R (79), followed by manual annotation of genotypes. Samples appeared to either cluster into groups of two or three genotypes. CNVr candidates displaying two clear genotypes were likely to have one rare homozygote, or the heterozygote and one homozygote class were indistinguishable. As such, we assigned k-values of either 2 or 3 depending on whether visual inspection indicated the presence of two or three segregating genotypes. To test for association between CNVrs overlapping or neighboring chromosomal inversions, we used the cor function in R (R team) to calculate correlations between CNVr and the genotypes of overlapping inversions that were previously identified by Battlay *et al.* (15). To visualize CNVrs that were heterozygous between haplotypes of the diploid reference genome, we aligned both reference haplotypes using minimap2 v2.1.8 (-k19 -w19 -m200) (80) and generated dotplots of the alignments. To call segregating SVs in the diploid reference, we aligned both haplotypes using nucmer (--maxmatch -c 100 -b 500 -l 50) within the mummer v3.23 software package (81). We then used SyRI (82) to identify and plotsr (-s 300000) (83) to visualize structural variants greater than 300 kbp in length. This method of identifying large segregating CNVs is constrained in that it can only identify CNVrs that contain a presence variant on haplotype 1 of the reference. Since haplotype 1 is larger than haplotype 2, it is more likely to contain more presence variants. Secondly, to create a strong signature of divergence within the local PCA, a large number of individuals must contain the absence variant, meaning that presence variants will also be rare. Furthermore, closer inspection of segregating CNVrs within the reference indicated that some CNVrs may consist of complex SVs, containing inversions and translocations, which our identification method using WGS failed to identify.

Since cnv-chr4a was surprisingly large and segregating in our diploid reference, we conducted further analyses to understand its genomic makeup. Firstly, we analyzed TE content within this region. We identified TEs using EDTA (84) and used RepeatMasker v4.1.1 (85) to obtain a summary of various TE families within this region relative to the rest of chromosome 4. We then performed a synteny analysis to determine if the small number of genes in that region were collinear with other genomic regions and were therefore an ancestral arrangement, or if they were novel combinations of genes. We used McScanX v97e74f4 (86) to determine syntenic gene groups resulting from a self-alignment of protein sequences on haplotype 1 using blastp (-evalue 1e-10) in BLAST v2.7.1 [87]). We calculated read-depth on chromosome 4 for three aligned *Ambrosia* outgroup species (30). Calculating

the mean read-depth exclusively within the cnv-chr4a region allowed us to ascertain the likely ancestral state of this structural variant.

Temporal CNV changes

To analyze shifts in CNV frequency over both time and space, we used generalized linear models with the glm function in R (88) to predict presence/absence counts in populations from range (Europe or North America), sample year and sample latitude, including significant interactions between the three variables. PC1, which was calculated from a covariance matrix of 10,000 SNPs randomly sampled from outside of genes and putative inversions identified by Battlay et al. (15), was included in each model to control for population structure. Model significance was tested with the anova function using a type-3 test (car v3.1-2 package [89]). The models were reduced in a stepwise fashion, removing non-significant interactions until all remaining interactions (if any) were significant ($p < 0.05$). The emtrends function (emmeans v1.10.2 package [90]) was used to test directionality and obtain confidence intervals within interacting predictors.

CNV-trait associations

To investigate associations between copy number variants and traits, we measured associations between 29 traits (in 121 samples for which trait data were available [41]) and the coverage windows described above. For each window, we fit linear models, using lm in R (88), between each sample's normalized window depth and each trait value. To account for population structure, the first principal component of neutral covariance was added to the model. As previously, this was obtained by calculating a covariance matrix on 10,000 putatively neutral sites that were outside gene and inversion regions using PCangsd. A PCA was performed on this covariance matrix using *prcomp* in R (88). We assessed significance using a Bonferroni-corrected significance threshold: 0.05 divided by the number of windows tested (17,855). We performed CNVr-trait associations using EMMAX (v.beta-7Mar2010 [91]) to identify associations between the CNV regions, using a covariance matrix consisting of the same 10,000 putatively neutral SNPs in previous analyses in this study to correct for population structure.

Gene Ontology analyses

Gene ontology enrichment analyses were performed using the R package topGO (92), using GO terms from *A. thaliana* TAIR 10 BLAST results. Fisher's exact test, using a significance

threshold of $p < 0.05$, was used to identify GO terms enriched within candidate gene lists relative to Q_{ST} outliers, as well as genes within CNVr.

References

1. R. A. Fisher, XV.—The Correlation between Relatives on the Supposition of Mendelian Inheritance. *Earth Environ. Sci. Trans. R. Soc. Edinb.* **52**, 399–433 (1919).
2. J. K. Pritchard, J. K. Pickrell, G. Coop, The Genetics of Human Adaptation: Hard Sweeps, Soft Sweeps, and Polygenic Adaptation. *Curr. Biol.* **20**, R208–R215 (2010).
3. A. E. Van't Hof, *et al.*, The industrial melanism mutation in British peppered moths is a transposable element. *Nature* **534**, 102–105 (2016).
4. A. J. Jensen, *et al.*, Large-effect loci mediate rapid adaptation of salmon body size after river regulation. *Proc. Natl. Acad. Sci.* **119**, e2207634119 (2022).
5. T. Connallon, K. A. Hodgins, Allen Orr and the genetics of adaptation. *Evolution* **75**, 2624–2640 (2021).
6. H. A. Orr, The Population Genetics of Adaptation: The Distribution of Factors Fixed During Adaptive Evolution. *Evolution* **52**, 935–949 (1998).
7. S. Yeaman, M. C. Whitlock, The genetic architecture of adaptation under migration-selection balance. *Evol. Int. J. Org. Evol.* **65**, 1897–1911 (2011).
8. P. Battlay, S. Yeaman, K. A. Hodgins, Impacts of pleiotropy and migration on repeated genetic adaptation. [Preprint] (2023). Available at: https://www.biorxiv.org/content/10.1101/2021.09.13.459985v5 [Accessed 2 June 2024].
9. M. Wellenreuther, L. Bernatchez, Eco-Evolutionary Genomics of Chromosomal Inversions. *Trends Ecol. Evol.* **33**, 427–440 (2018).
10. M. Chakraborty, J. J. Emerson, S. J. Macdonald, A. D. Long, Structural variants exhibit widespread allelic heterogeneity and shape variation in complex traits. *Nat. Commun.* **10**, 4872 (2019).
11. A. H. Sturtevant, A Case of Rearrangement of Genes in Drosophila. *Proc. Natl. Acad. Sci. U. S. A.* **7**, 235–237 (1921).
12. T. Dobzhansky, *Genetics of the Evolutionary Process* (Columbia University Press, 1970).
13. H. Cayuela, *et al.*, Thermal adaptation rather than demographic history drives genetic structure inferred by copy number variants in a marine fish. *Mol. Ecol.* **30**, 1624–1641 (2021).
14. C. K. Tepolt, E. D. Grosholz, C. E. de Rivera, G. M. Ruiz, Balanced polymorphism fuels rapid selection in an invasive crab despite high gene flow and low genetic diversity. *Mol. Ecol.* **31**, 55–69 (2022).
15. P. Battlay, *et al.*, Large haploblocks underlie rapid adaptation in the invasive weed Ambrosia artemisiifolia. *Nat. Commun.* **14**, 1717 (2023).
16. M. M. Magwire, F. Bayer, C. L. Webster, C. Cao, F. M. Jiggins, Successive Increases in the Resistance of Drosophila to Viral Infection through a Transposon Insertion Followed by a Duplication. *PLOS Genet.* **7**, e1002337 (2011).
17. E. R. Lucas, *et al.*, Whole-genome sequencing reveals high complexity of copy number

variation at insecticide resistance loci in malaria mosquitoes. *Genome Res.* **29**, 1250–1261 (2019).
18. S. DeBolt, Copy number variation shapes genome diversity in Arabidopsis over immediate family generational scales. *Genome Biol. Evol.* **2**, 441–453 (2010).
19. T. A. Gaines, *et al.*, Gene amplification confers glyphosate resistance in Amaranthus palmeri. *Proc. Natl. Acad. Sci.* **107**, 1029–1034 (2010).
20. P. J. Daborn, *et al.*, A single p450 allele associated with insecticide resistance in Drosophila. *Science* **297**, 2253–2256 (2002).
21. R. H. Ffrench-Constant, The molecular genetics of insecticide resistance. *Genetics* **194**, 807–815 (2013).
22. C. Zhang, *et al.*, Investigating the mechanisms of glyphosate resistance in goosegrass (*Eleusine indica*) population from South China. *J. Integr. Agric.* **14**, 909–918 (2015).
23. J. M. Kreiner, *et al.*, Multiple modes of convergent adaptation in the spread of glyphosate-resistant Amaranthus tuberculatus. *Proc. Natl. Acad. Sci.* **116**, 21076–21084 (2019).
24. N. M. Reid, *et al.*, The genomic landscape of rapid repeated evolutionary adaptation to toxic pollution in wild fish. *Science* **354**, 1305–1308 (2016).
25. S. Gimenez, *et al.*, Adaptation by copy number variation increases insecticide resistance in the fall armyworm. *Commun. Biol.* **3**, 664 (2020).
26. J. Prunier, *et al.*, Gene copy number variations involved in balsam poplar (Populus balsamifera L.) adaptive variations. *Mol. Ecol.* **28**, 1476–1490 (2019).
27. Y. Dorant, *et al.*, Copy number variants outperform SNPs to reveal genotype–temperature association in a marine species. *Mol. Ecol.* **29**, 4765–4782 (2020).
28. K. A. Hodgins, D. G. Bock, L. H. Rieseberg, "Trait Evolution in Invasive Species" in *Annual Plant Reviews Online*, (John Wiley & Sons, Ltd, 2018), pp. 459–496.
29. R. I. Colautti, S. C. H. Barrett, Rapid Adaptation to Climate Facilitates Range Expansion of an Invasive Plant. *Science* **342**, 364–366 (2013).
30. V. C. Bieker, *et al.*, Uncovering the genomic basis of an extraordinary plant invasion. *Sci. Adv.* **8**, eabo5115 (2022).
31. A. McGaughran, *et al.*, Genomic Tools in Biological Invasions: Current State and Future Frontiers. *Genome Biol. Evol.* **16**, evad230 (2024).
32. D. B. Stern, C. E. Lee, Evolutionary origins of genomic adaptations in an invasive copepod. *Nat. Ecol. Evol.* **4**, 1084–1094 (2020).
33. L. A. van Boheemen, K. A. Hodgins, Rapid repeatable phenotypic and genomic adaptation following multiple introductions. *Mol. Ecol.* **29**, 4102–4117 (2020).
34. K. M. Dlugosch, S. R. Anderson, J. Braasch, F. A. Cang, H. D. Gillette, The devil is in the details: genetic variation in introduced populations and its contributions to invasion. *Mol. Ecol.* **24**, 2095–2111 (2015).
35. A. Estoup, *et al.*, Is There a Genetic Paradox of Biological Invasion? *Annu. Rev. Ecol. Evol. Syst.* **47**, 51–72 (2016).
36. F. Essl, *et al.*, Biological Flora of the British Isles: Ambrosia artemisiifolia. *J. Ecol.* **103**, 1069–1098 (2015).
37. U. Schaffner, *et al.*, Biological weed control to relieve millions from Ambrosia allergies in Europe. *Nat. Commun.* **11**, 1745 (2020).
38. M. J. Cowbrough, R. B. Brown, F. J. Tardif, Impact of common ragweed (Ambrosia artemisiifolia) aggregation on economic thresholds in soybean. *Weed Sci.* **51**, 947–954 (2003).
39. C. E. Brewer, L. R. Oliver, Confirmation and Resistance Mechanisms in Glyphosate-Resistant Common Ragweed (Ambrosia artemisiifolia) in Arkansas. *Weed Sci.* **57**, 567–573 (2009).

40. L. A. van Boheemen, *et al.*, Multiple introductions, admixture and bridgehead invasion characterize the introduction history of Ambrosia artemisiifolia in Europe and Australia. *Mol. Ecol.* **26**, 5421–5434 (2017).
41. L. A. van Boheemen, D. Z. Atwater, K. A. Hodgins, Rapid and repeated local adaptation to climate in an invasive plant. *New Phytol.* **222**, 614–627 (2019).
42. A. J. Gorton, D. A. Moeller, P. Tiffin, Little plant, big city: a test of adaptation to urban environments in common ragweed (Ambrosia artemisiifolia). *Proc. R. Soc. B Biol. Sci.* **285**, 20180968 (2018).
43. Y. Sun, G. K. Roderick, Rapid evolution of invasive traits facilitates the invasion of common ragweed, Ambrosia artemisiifolia. *J. Ecol.* **107**, 2673–2687 (2019).
44. B. V. McGoey, J. R. Stinchcombe, Introduced populations of ragweed show as much evolutionary potential as native populations. *Evol. Appl.* **14**, 1436–1449 (2021).
45. R. C. Lewontin, J. Krakauer, DISTRIBUTION OF GENE FREQUENCY AS A TEST OF THE THEORY OF THE SELECTIVE NEUTRALITY OF POLYMORPHISMS. *Genetics* **74**, 175–195 (1973).
46. B. S. Weir, C. C. Cockerham, Estimating F-Statistics for the Analysis of Population Structure. *Evolution* **38**, 1358–1370 (1984).
47. M. C. Whitlock, Evolutionary inference from QST. *Mol. Ecol.* **17**, 1885–1896 (2008).
48. S. E. Fick, R. J. Hijmans, WorldClim 2: new 1-km spatial resolution climate surfaces for global land areas. *Int. J. Climatol.* **37**, 4302–4315 (2017).
49. B. J. Adamczyk, D. E. Fernandez, MIKC* MADS Domain Heterodimers Are Required for Pollen Maturation and Tube Growth in Arabidopsis. *Plant Physiol.* **149**, 1713–1723 (2009).
50. D. R. Schrider, M. W. Hahn, D. J. Begun, Parallel Evolution of Copy-Number Variation across Continents in Drosophila melanogaster. *Mol. Biol. Evol.* **33**, 1308–1316 (2016).
51. E. L. Patterson, D. J. Pettinga, K. Ravet, P. Neve, T. A. Gaines, Glyphosate Resistance and EPSPS Gene Duplication: Convergent Evolution in Multiple Plant Species. *J. Hered.* **109**, 117–125 (2018).
52. R. T. Good, *et al.*, The Molecular Evolution of Cytochrome P450 Genes within and between Drosophila Species. *Genome Biol. Evol.* **6**, 1118–1134 (2014).
53. G. van Ooijen, *et al.*, Structure-function analysis of the NB-ARC domain of plant disease resistance proteins. *J. Exp. Bot.* **59**, 1383–1397 (2008).
54. A. Żmieńko, A. Samelak, P. Kozłowski, M. Figlerowicz, Copy number polymorphism in plant genomes. *Theor. Appl. Genet.* **127**, 1–18 (2014).
55. A. Dolatabadian, D. A. Patel, D. Edwards, J. Batley, Copy number variation and disease resistance in plants. *Theor. Appl. Genet.* **130**, 2479–2490 (2017).
56. M. Todesco, *et al.*, Massive haplotypes underlie ecotypic differentiation in sunflowers. *Nature* **584**, 602–607 (2020).
57. C. Mérot, *et al.*, Genome assembly, structural variants, and genetic differentiation between lake whitefish young species pairs (Coregonus sp.) with long and short reads. *Mol. Ecol.* **32**, 1458–1477 (2023).
58. T. Hämälä, *et al.*, Genomic structural variants constrain and facilitate adaptation in natural populations of Theobroma cacao , the chocolate tree. *Proc. Natl. Acad. Sci.* **118**, e2102914118 (2021).
59. J. B. Koch, *et al.*, Population genomic and phenotype diversity of invasive Drosophila suzukii in Hawai‘i. *Biol. Invasions* **22**, 1753–1770 (2020).
60. N. R. Hofmeister, S. J. Werner, I. J. Lovette, Environmental correlates of genetic variation in the invasive European starling in North America. *Mol. Ecol.* **30**, 1251–1263 (2021).
61. T. Lin, P. G. L. Klinkhamer, K. Vrieling, Parallel evolution in an invasive plant: effect

of herbivores on competitive ability and regrowth of Jacobaea vulgaris. *Ecol. Lett.* **18**, 668–676 (2015).
62. K. C. Stuart, W. B. Sherwin, R. J. Edwards, L. A. Rollins, Evolutionary genomics: Insights from the invasive European starlings. *Front. Genet.* **13** (2023).
63. J. Ebler, *et al.*, Pangenome-based genome inference allows efficient and accurate genotyping across a wide spectrum of variant classes. *Nat. Genet.* **54**, 518–525 (2022).
64. B. Chauvel, F. Dessaint, C. Cardinal-Legrand, F. Bretagnolle, The historical spread of Ambrosia artemisiifolia L. in France from herbarium records. *J. Biogeogr.* **33**, 665–673 (2006).
65. M. J. Case, K. A. Stinson, Climate change impacts on the distribution of the allergenic plant, common ragweed (Ambrosia artemisiifolia) in the eastern United States. *PLOS ONE* **13**, e0205677 (2018).
66. J. M. Kreiner, S. Hnatovska, J. R. Stinchcombe, S. I. Wright, Quantifying the role of genome size and repeat content in adaptive variation and the architecture of flowering time in Amaranthus tuberculatus. *PLOS Genet.* **19**, e1010865 (2023).
67. M. Schubert, *et al.*, Characterization of ancient and modern genomes by SNP detection and phylogenomic and metagenomic analysis using PALEOMIX. *Nat. Protoc.* **9**, 1056–1082 (2014).
68. M. A. DePristo, *et al.*, A framework for variation discovery and genotyping using next-generation DNA sequencing data. *Nat. Genet.* **43**, 491–498 (2011).
69. P. Danecek, *et al.*, Twelve years of SAMtools and BCFtools. *GigaScience* **10**, giab008 (2021).
70. G. Coop, D. Witonsky, A. Di Rienzo, J. K. Pritchard, Using Environmental Correlations to Identify Loci Underlying Local Adaptation. *Genetics* **185**, 1411–1423 (2010).
71. M. Gautier, Genome-Wide Scan for Adaptive Divergence and Association with Population-Specific Covariates. *Genetics* **201**, 1555–1579 (2015).
72. K. Spitze, Population structure in Daphnia obtusa: quantitative genetic and allozymic variation. *Genetics* **135**, 367–374 (1993).
73. T. Prout, J. S. Barker, F statistics in Drosophila buzzatii: selection, population size and inbreeding. *Genetics* **134**, 369–375 (1993).
74. D. Bates, M. Mächler, B. Bolker, S. Walker, Fitting Linear Mixed-Effects Models Using lme4. *J. Stat. Softw.* **67**, 1–48 (2015).
75. P. Danecek, *et al.*, The variant call format and VCFtools. *Bioinformatics* **27**, 2156–2158 (2011).
76. H. Li, P. Ralph, Local PCA Shows How the Effect of Population Structure Differs Along the Genome. *Genetics* **211**, 289–304 (2019).
77. T. S. Korneliussen, A. Albrechtsen, R. Nielsen, ANGSD: Analysis of Next Generation Sequencing Data. *BMC Bioinformatics* **15**, 356 (2014).
78. J. Meisner, A. Albrechtsen, Inferring Population Structure and Admixture Proportions in Low-Depth NGS Data. *Genetics* **210**, 719–731 (2018).
79. L. Mouselimis, *et al.*, ClusterR: Gaussian Mixture Models, K-Means, Mini-Batch-Kmeans, K-Medoids and Affinity Propagation Clustering. (2023). Deposited 4 December 2023.
80. H. Li, Minimap2: pairwise alignment for nucleotide sequences. *Bioinformatics* **34**, 3094–3100 (2018).
81. S. Kurtz, *et al.*, Versatile and open software for comparing large genomes. *Genome Biol.* **5**, R12 (2004).
82. M. Goel, H. Sun, W.-B. Jiao, K. Schneeberger, SyRI: finding genomic rearrangements and local sequence differences from whole-genome assemblies. *Genome Biol.* **20**, 277 (2019).

83. M. Goel, K. Schneeberger, plotsr: visualizing structural similarities and rearrangements between multiple genomes. *Bioinformatics* **38**, 2922–2926 (2022).
84. S. Ou, *et al.*, Benchmarking transposable element annotation methods for creation of a streamlined, comprehensive pipeline. *Genome Biol.* **20**, 275 (2019).
85. Smit, AFA, Hubley, R & Green, P., RepeatMasker Open-4.0. 2013-2015 <http://www.repeatmasker.org>.
86. Y. Wang, *et al.*, MCScanX: a toolkit for detection and evolutionary analysis of gene synteny and collinearity. *Nucleic Acids Res.* **40**, e49 (2012).
87. C. Camacho, *et al.*, BLAST+: architecture and applications. *BMC Bioinformatics* **10**, 421 (2009).
88. R Foundation for Statistical Computing, Vienna, Austria., R: A language and environment for statistical computing. (2024). Deposited 2024.
89. J. Fox, S. Weisberg, *An R Companion to Applied Regression*, Third (Sage, 2019).
90. R. V. Lenth, *et al.*, emmeans: Estimated Marginal Means, aka Least-Squares Means. (2024). Deposited 23 January 2024.
91. H. M. Kang, *et al.*, Variance component model to account for sample structure in genome-wide association studies. *Nat. Genet.* **42**, 348–354 (2010).
92. A. Alexa, J. Rahnenführer, Gene set enrichment analysis with topGO.

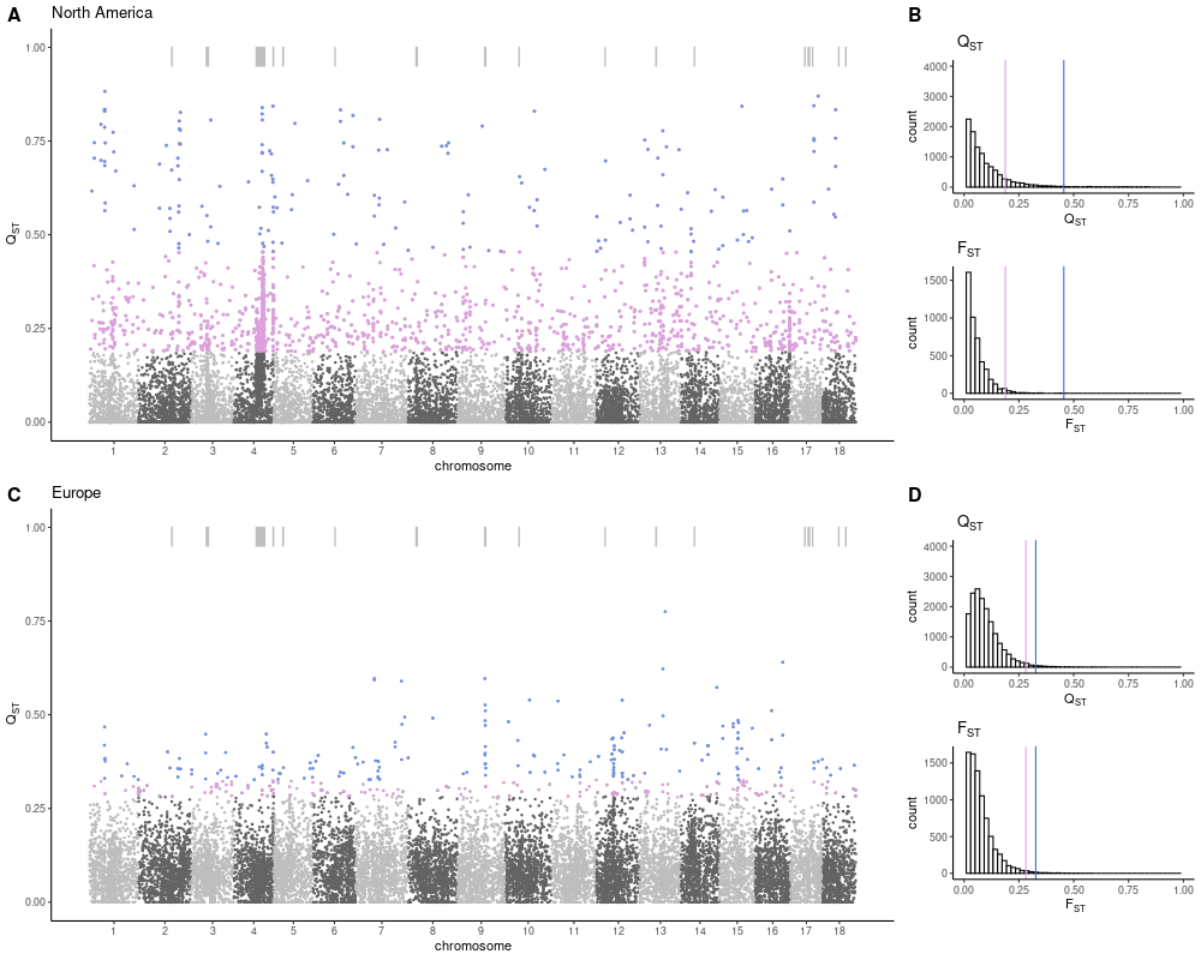

Figure 1. CNV Q_{ST} values indicate regions of selection in the A. artemisiifolia genome. A. Q_{ST} values of filtered coverage windows in European populations. Pink windows indicate those above 1% F_{ST} threshold shown in **B**, blue windows indicate top 1% of Q_{ST} values. **C.** Q_{ST} values of filtered coverage windows in North American populations. Pink windows indicate those above 1% F_{ST} threshold shown in **D**, blue windows indicate top 1% of Q_{ST} values. Bars above manhattan plots indicate merged windows > 300 kbp.

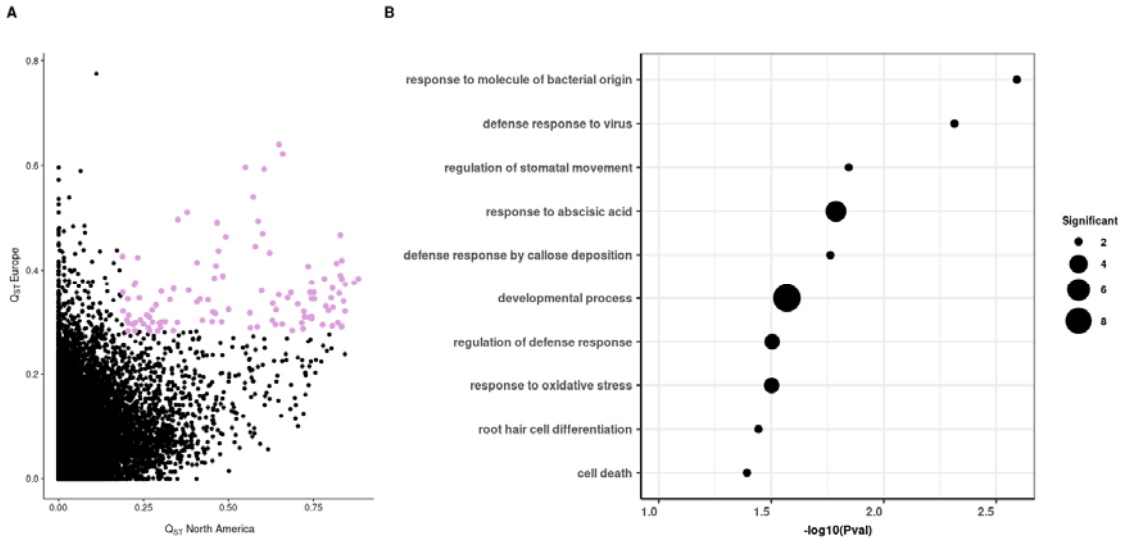

Figure 2. Overlapping Q_{ST} outliers in both ranges and their potential biological functions. A. Distribution of Q_{ST} values of all 10 kbp coverage windows in both North America and Europe. Overlapping windows exceeding the neutral F_{ST} threshold of 1% in each respective range are colored in pink. **B.** Gene ontology enrichment plot of genes within overlapping outlier Q_{ST} windows, with biological pathways only retained if represented by 2 or more genes (pink in **A**).

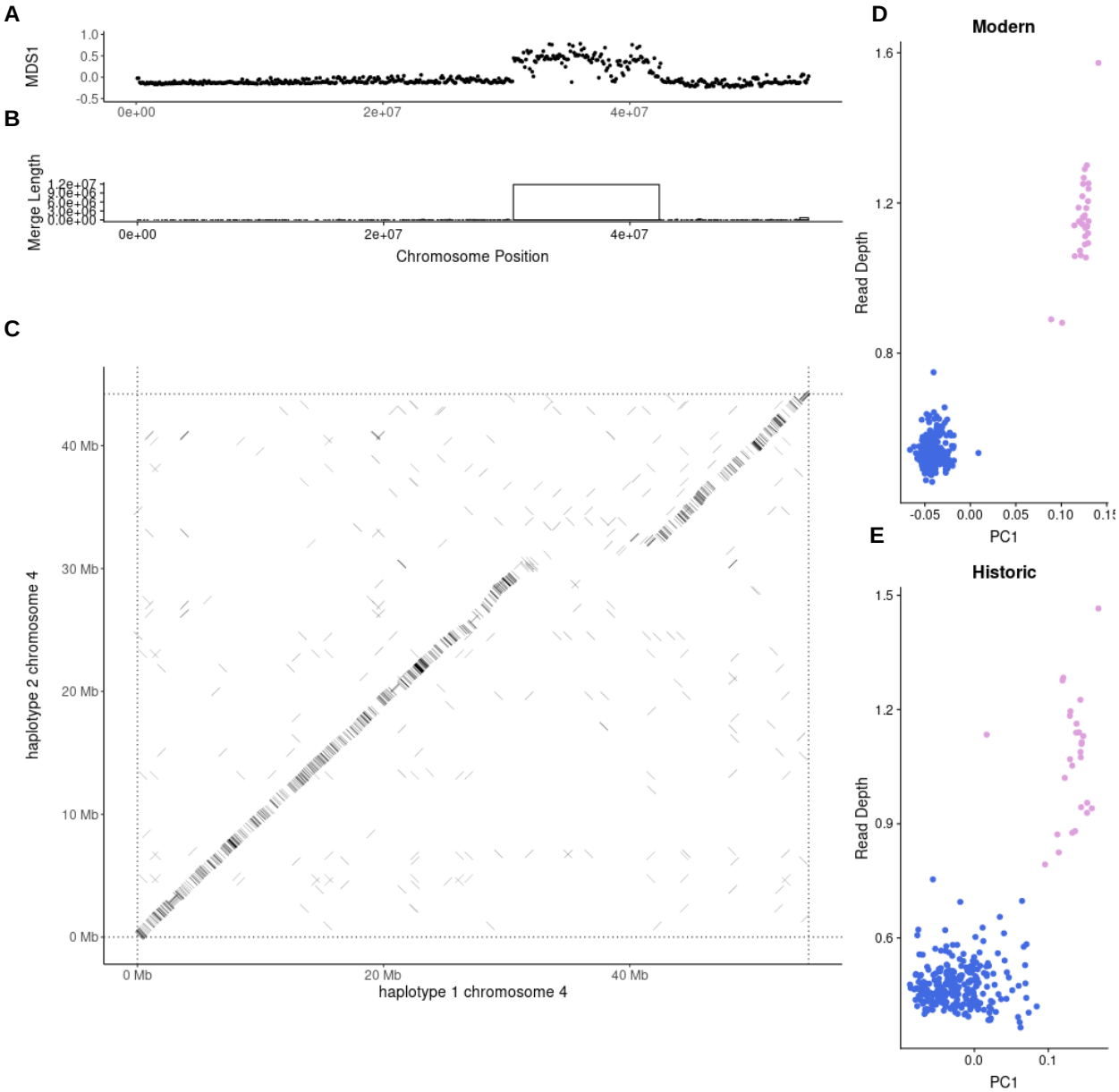

Figure 3. CNVr genotyping of cnv-chr4a. A. MDS coordinates from local PCA in 100kb windows across chromosome 4. Values diverging from zero indicate local structure compared with the rest of the chromosome. **B.** Distribution of merged window sizes along chromosome 4, with boxes indicating window size on the Y axis and chromosomal position on the X axis. **C.** Alignment of chromosome 4 Hap1 and Hap2 of the diploid reference genome. A clear gap is present corresponding to local PCA and merged window locations. **D**, **E**. Regional PC1 against regional read-depth corresponding to merged window identified in **B.** Clustering computed using k-means and manual annotation. **D**. represents modern samples and **E.** represents historic samples.

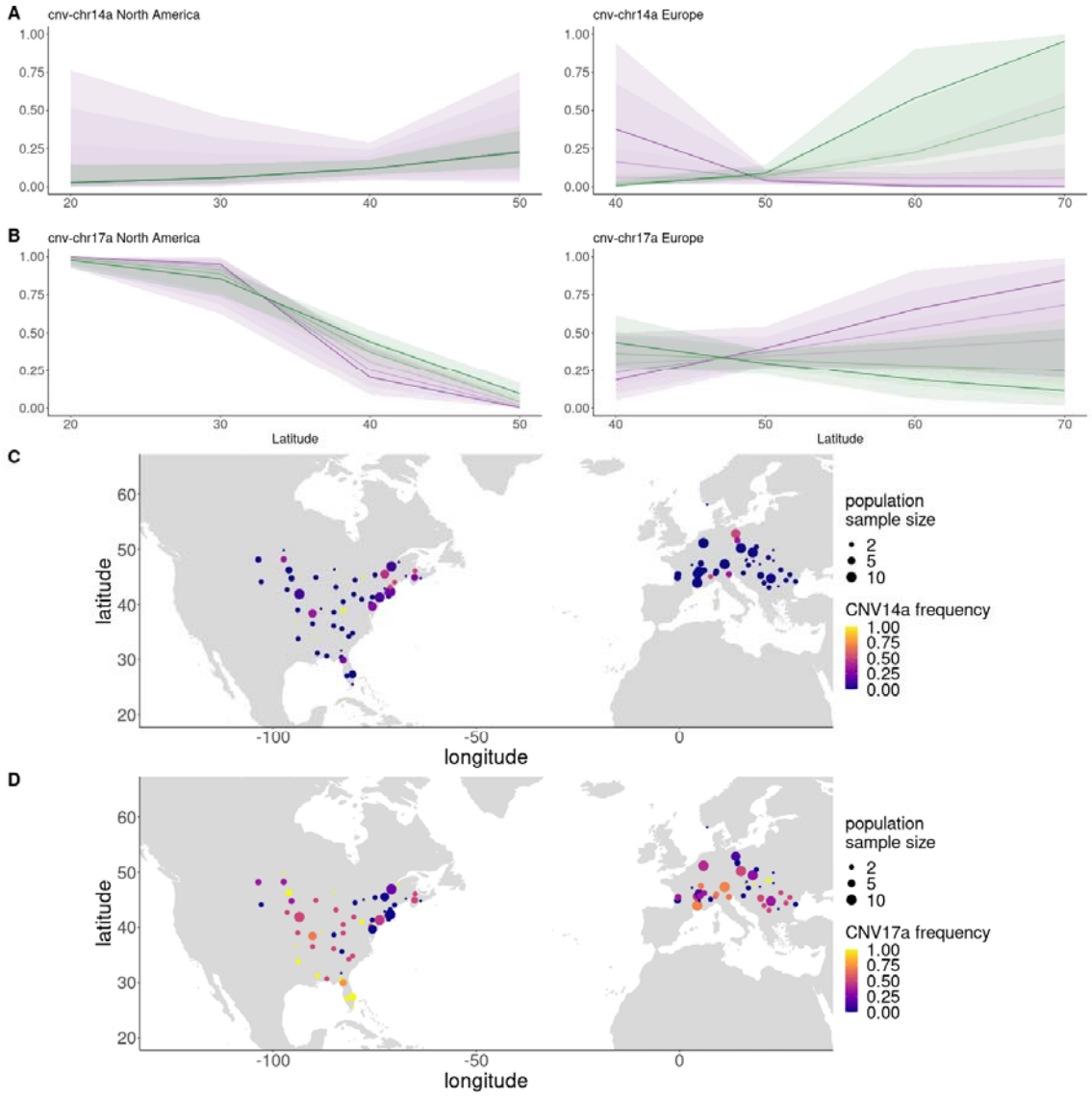

Figure 4. Spatio-temporal CNV frequency shifts. A. Logistic regression models for cnv-chr14a and cnv-chr-10a with error bands representing 95% CI of least-squares regressions of CNV frequency. Time binned into five categories, ranging from historic (purple) to modern (green). Model information found in Supplementary Table 6. **B.** Frequency of CNV17a in modern A. artemisiifolia populations.

Supplementary figures

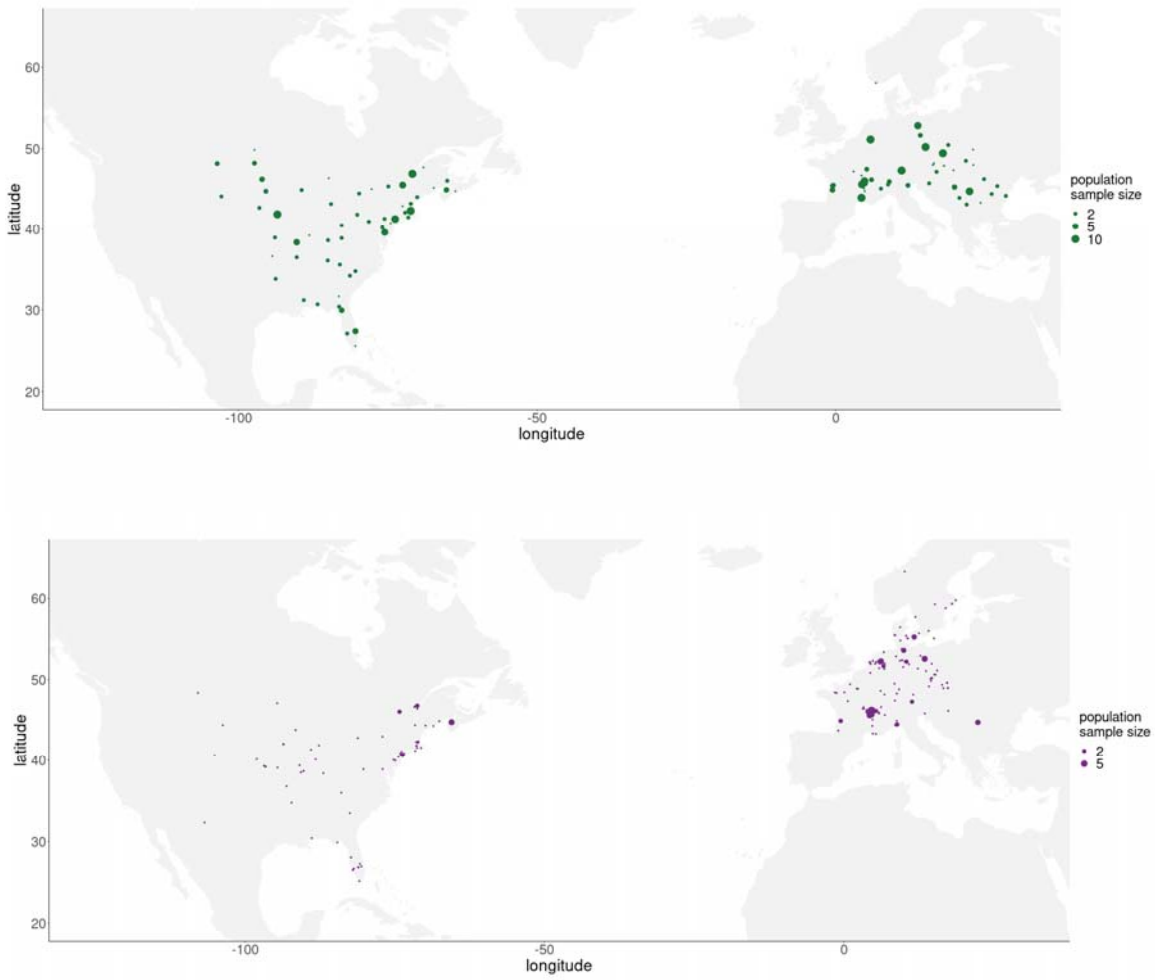

Supplementary Figure 1. Sampling locations of Ambrosia artemisiifolia.

A. Modern sampling locations. **B.** Historic sampling locations

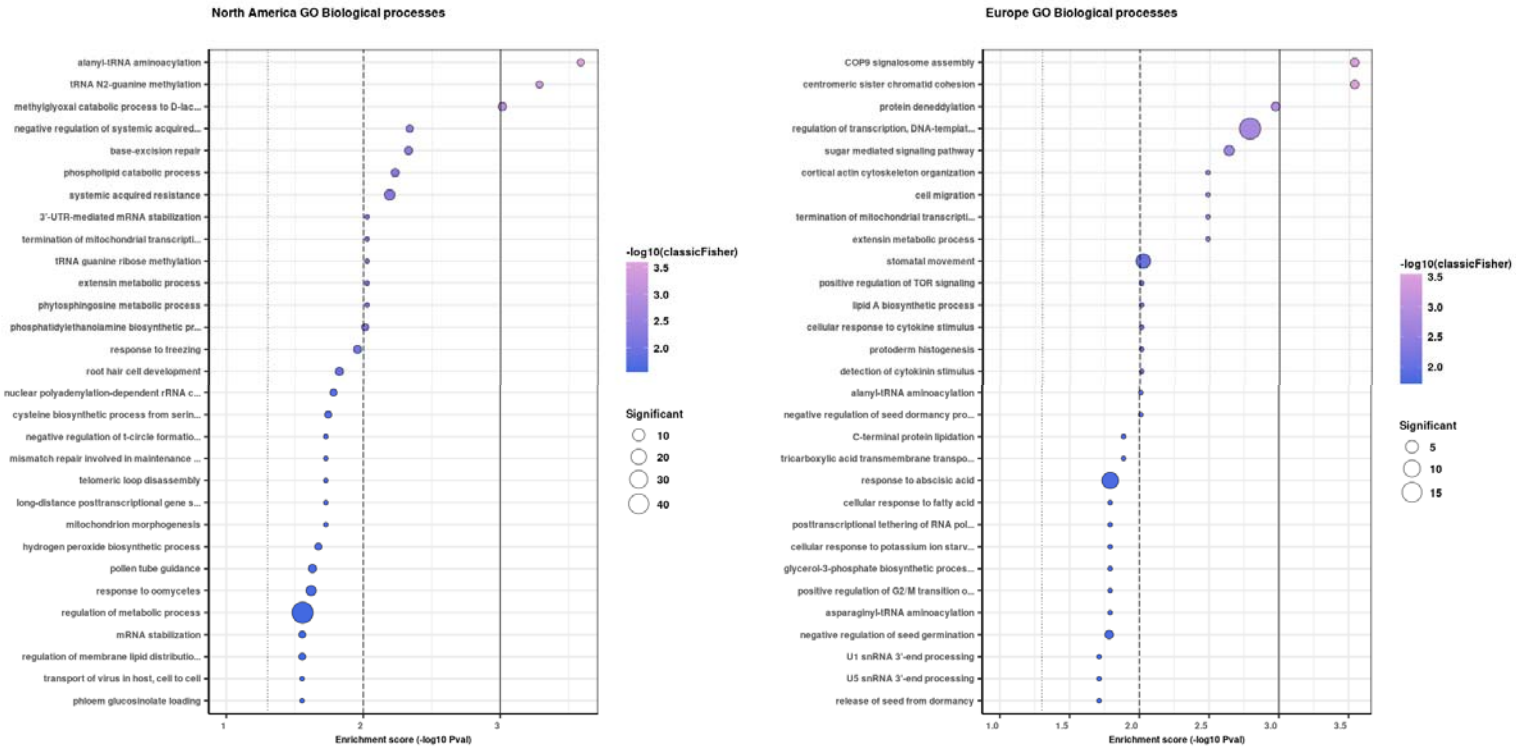

Supplementary Figure 2. Gene ontology enrichment analysis for Q_{ST} outliers in each range.

A. Gene ontology enrichment plot of genes within overlapping outlier North American Q_{ST} windows, with biological pathways only retained if represented by 2 or more genes. **B.** Gene ontology enrichment plot of genes within overlapping outlier European Q_{ST} windows, with biological pathways only retained if represented by 2 or more genes.

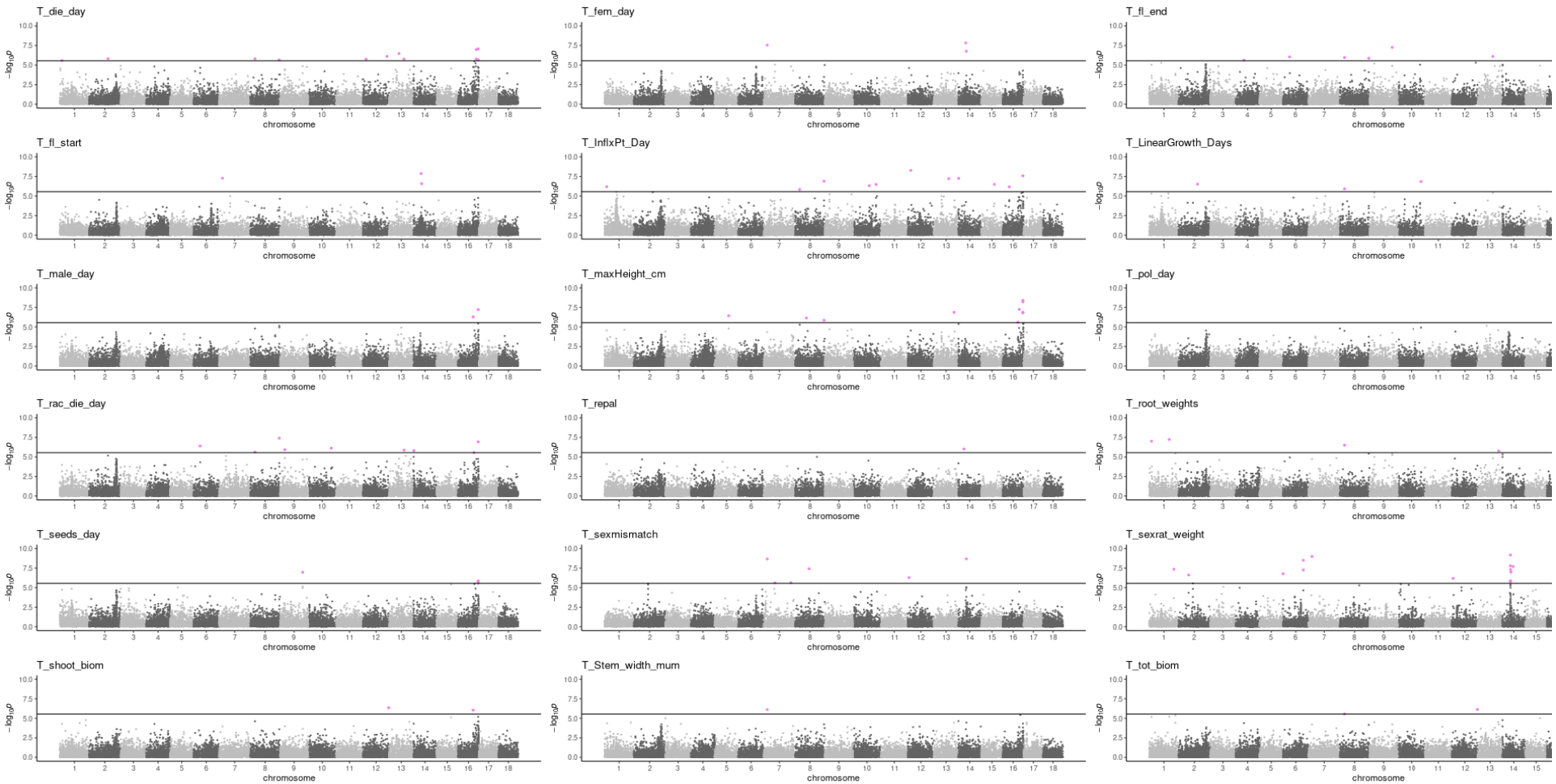

Supplementary Figure 3. Coverage window associations with traits.

Manhattan plots of P-values from linear models performed for each coverage window within 121 samples with trait data against 18 traits. Pink values represent bonferroni-significant associations. Trait information in Supplementary Table 5.

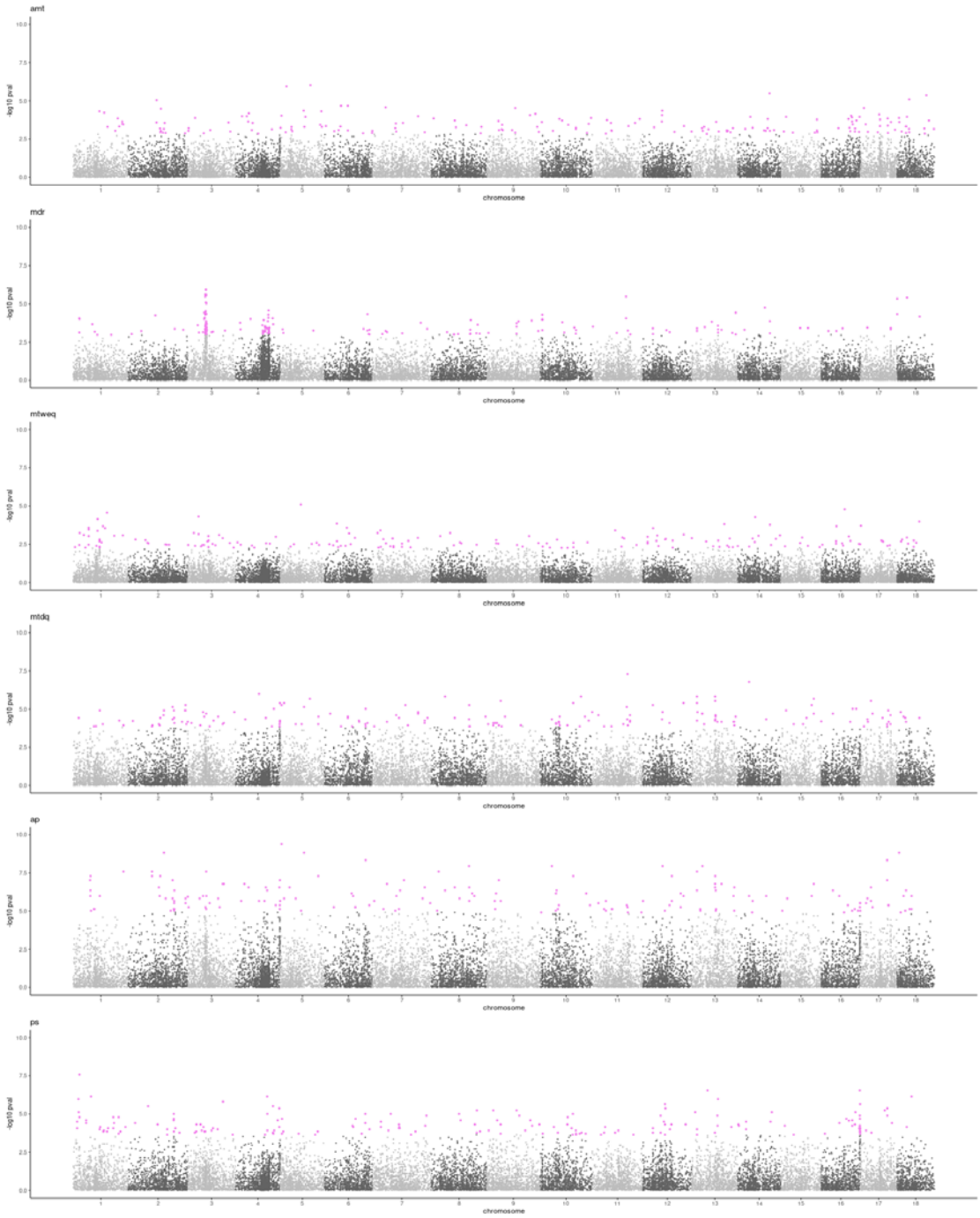

Supplementary Figure 4. Coverage window associations with bioclimatic variables in North American range.

Bioclimatic variables included are those after filtering for associations with other variables >= R 0.7. Associations performed using Spearman's Rho. P-values calculated according to empirical distribution of Rho values (amt: annual mean temperature; mdr: mean diurnal range; mtweq: mean temperature of wettest quarter; mtdq: mean temperature of driest quarter; ap: annual precipitation; ps: precipitation seasonality).

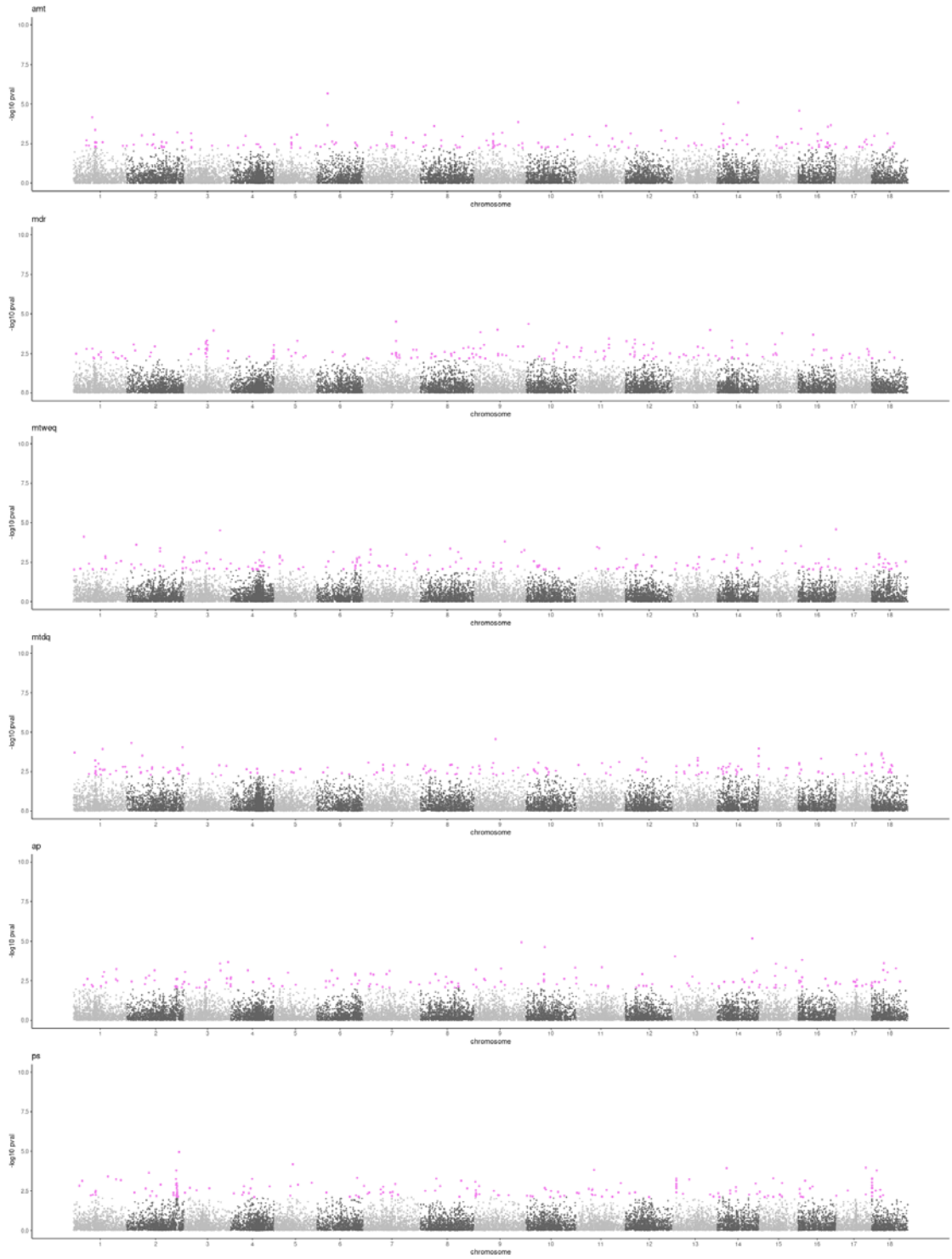

Supplementary Figure 5. Coverage window associations with bioclimatic variables in European range. Bioclimatic variables included are those after filtering for associations with other variables >= R 0.7. Associations performed using Spearman's Rho. P-values calculated according to empirical distribution of Rho values (amt: annual mean temperature; mdr: mean diurnal range; mtweq: mean temperature of wettest quarter; mtdq: mean temperature of driest quarter; ap: annual precipitation; ps: precipitation seasonality).

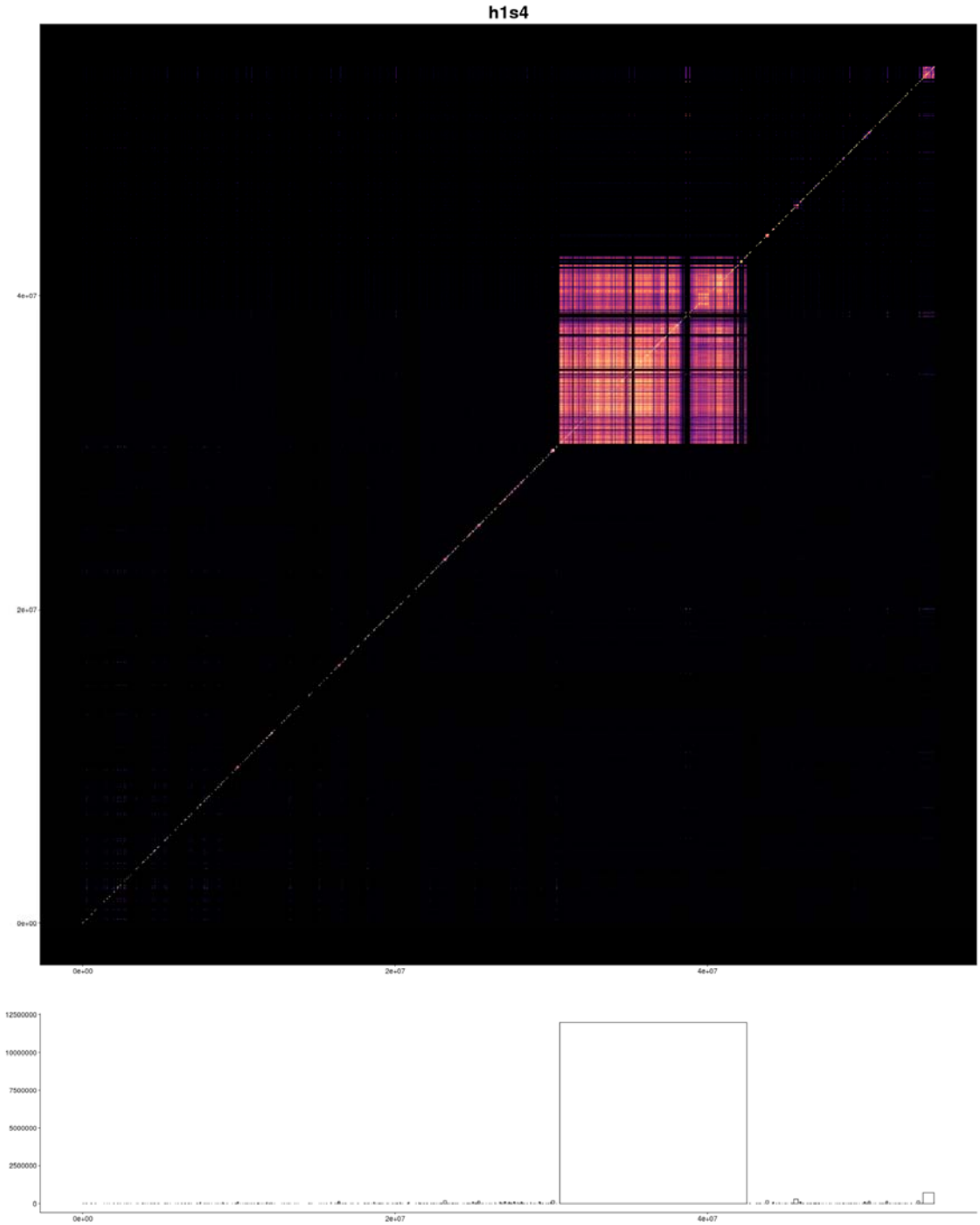
h1s4
4e+07
2e+07
0e+00
0e+00
2e+07
4e+07
12500000
10000000
7500000
5000000
2500000
0
0e+00
2e+07
4e+07

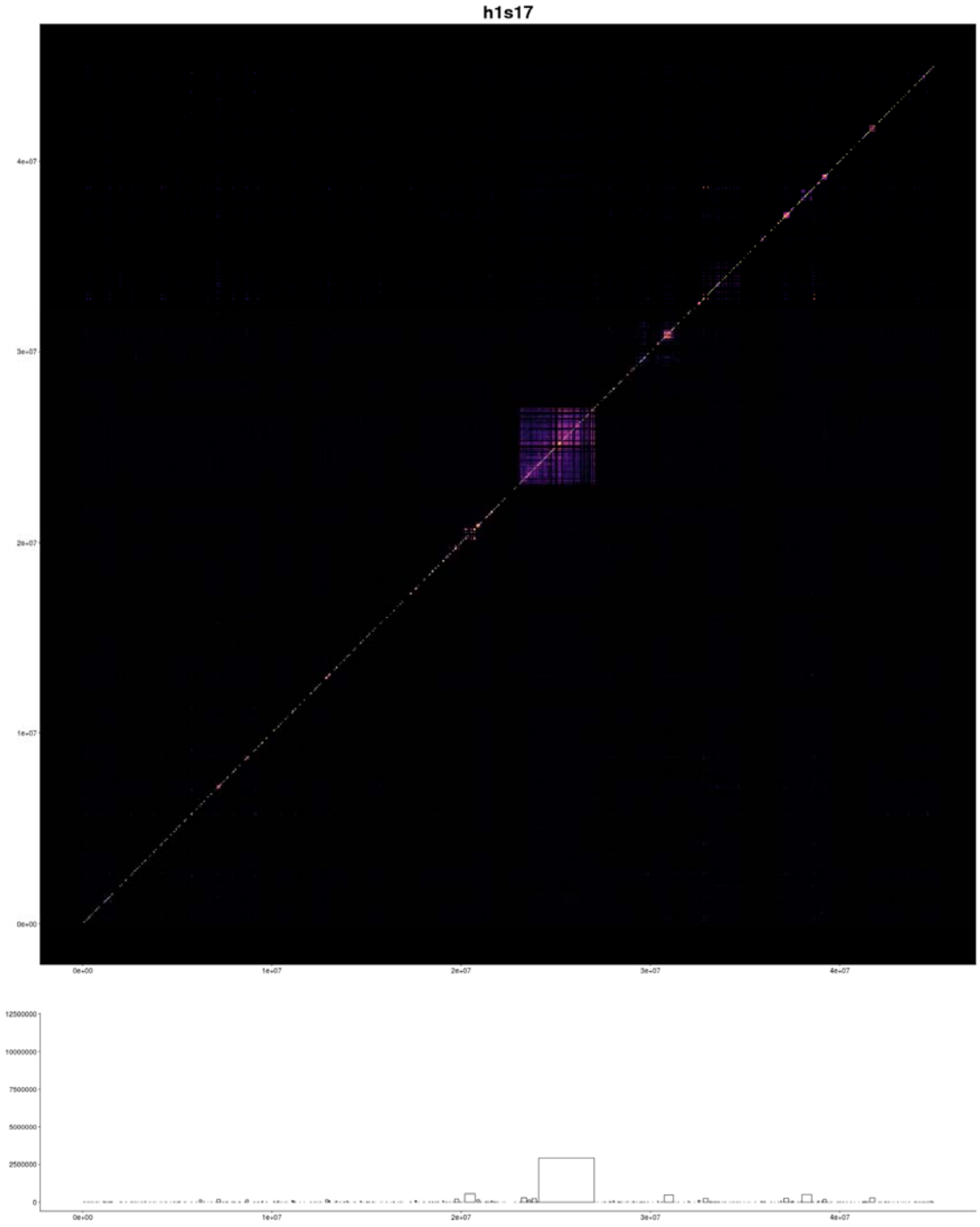

Supplementary Figure 6. Candidate CNV window merging. Top panels are heat maps representing correlations of standardized read-depth in the 10 kbp windows on each chromosome. Lighter colors indicate greater correlation. Bottom panels indicate locations of merged CNVs (windows within 1 Mbp where read-depth R2 exceeded 0.6). X-axis represents chromosome coordinates, and Y-axis indicates size of merged CNVs.

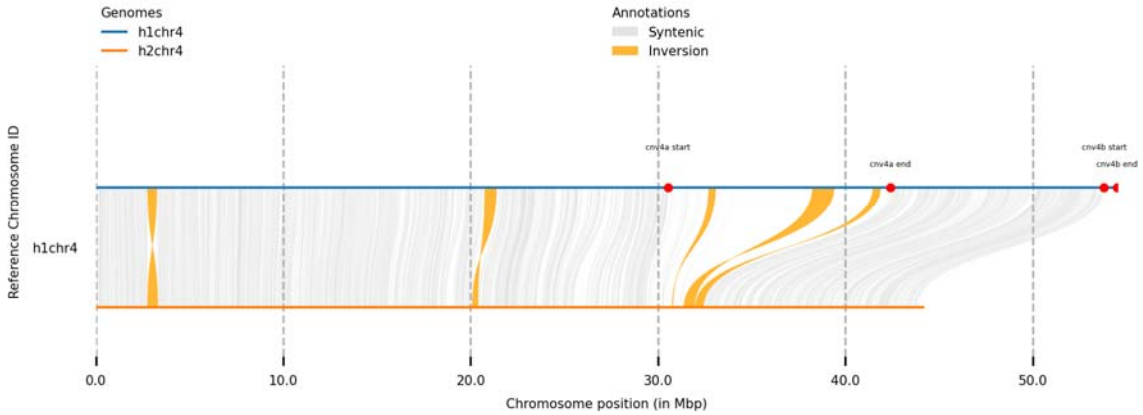

Supplementary Figure 7. Structural variation in chromosome 4 in *A. artemisiifolia* diploid reference. Structural variants between haplotype 1 and haplotype 2 of reference detected with SyRI (82). Inversions represented by orange bands and syntenic regions represented by gray bands. Red dots indicate boundaries of CNVr on chromosome 4.

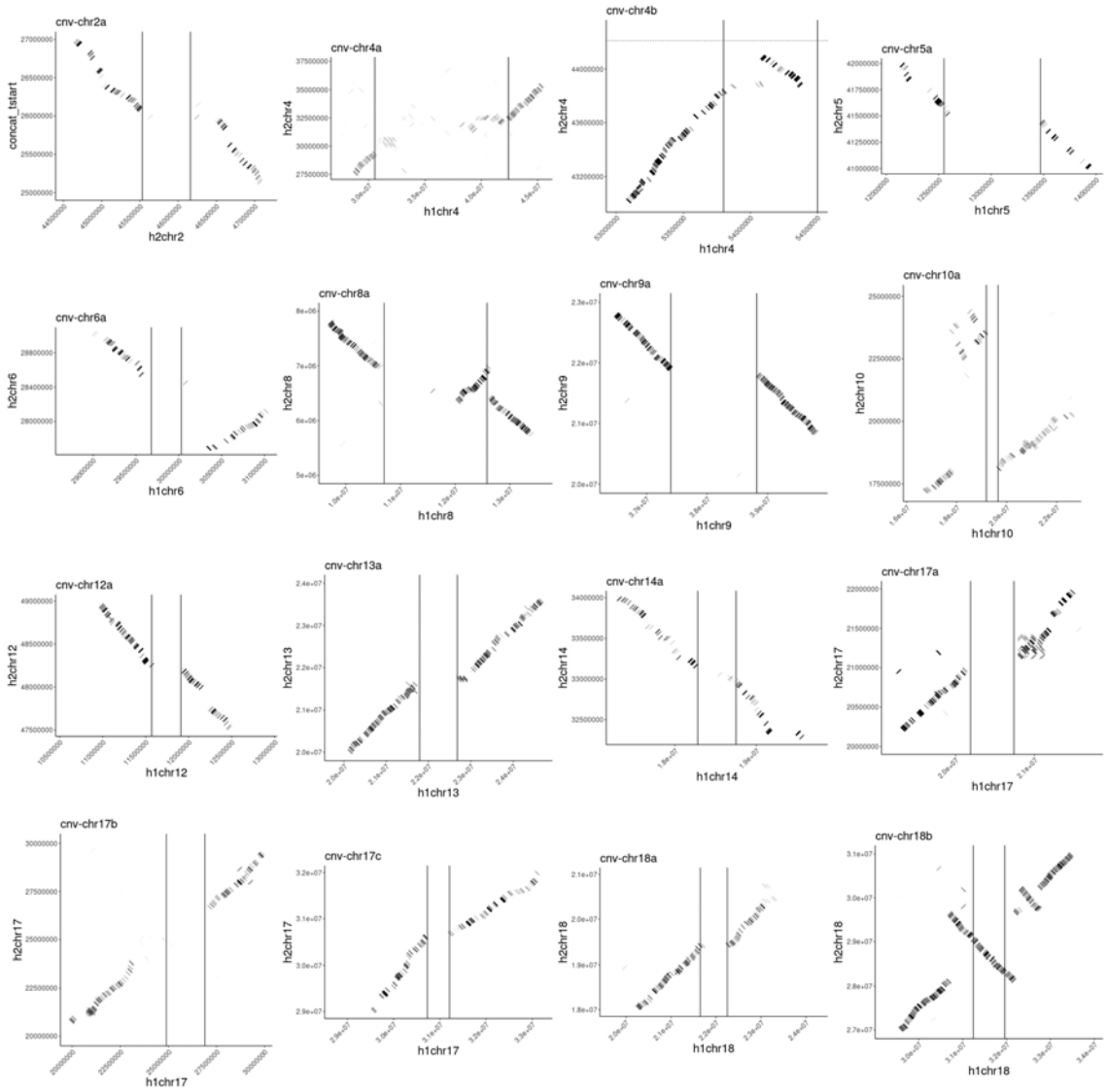

Supplementary Figure 8. *A. artemisiifolia* reference genome alignments zoomed in on CNV regions. Dotplots of alignments performed using minimap2 between both haplotypes of the diploid reference genome (15), zoomed in on regions containing CNVrs. CNVr start and end points denoted by vertical lines.

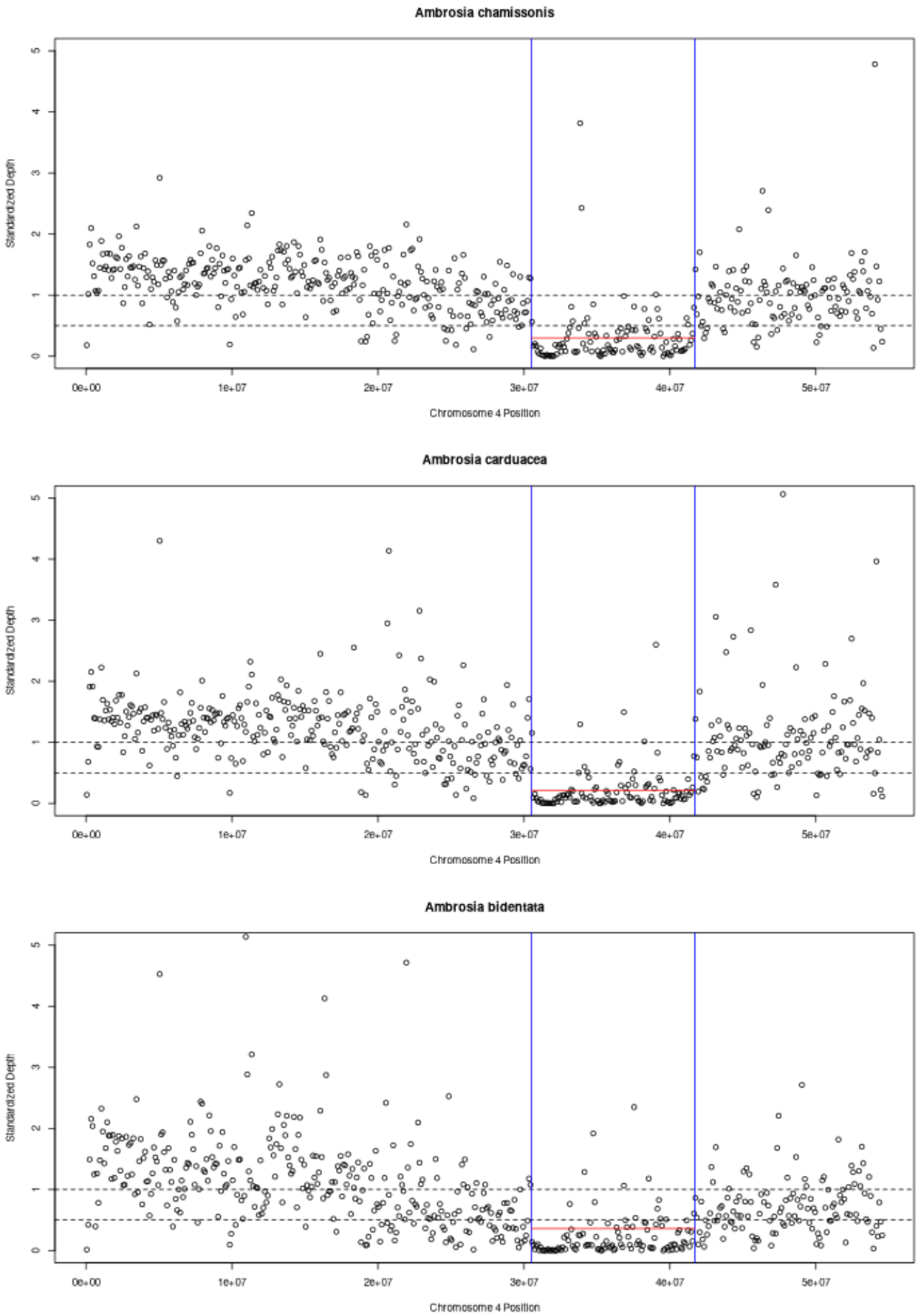

Supplementary Figure 9. Read-depth along chromosome 4 of 10 Ambrosia outgroup species mapped to *A. artemisiifolia* haplotype 1 reference genome. Vertical blue lines denote the starts and ends of cnv-chr4a. Horizontal red lines indicate average read-depth within the cnv-chr4a region. Details of *Ambrosia* outgroup species in Bieker et al. (30).

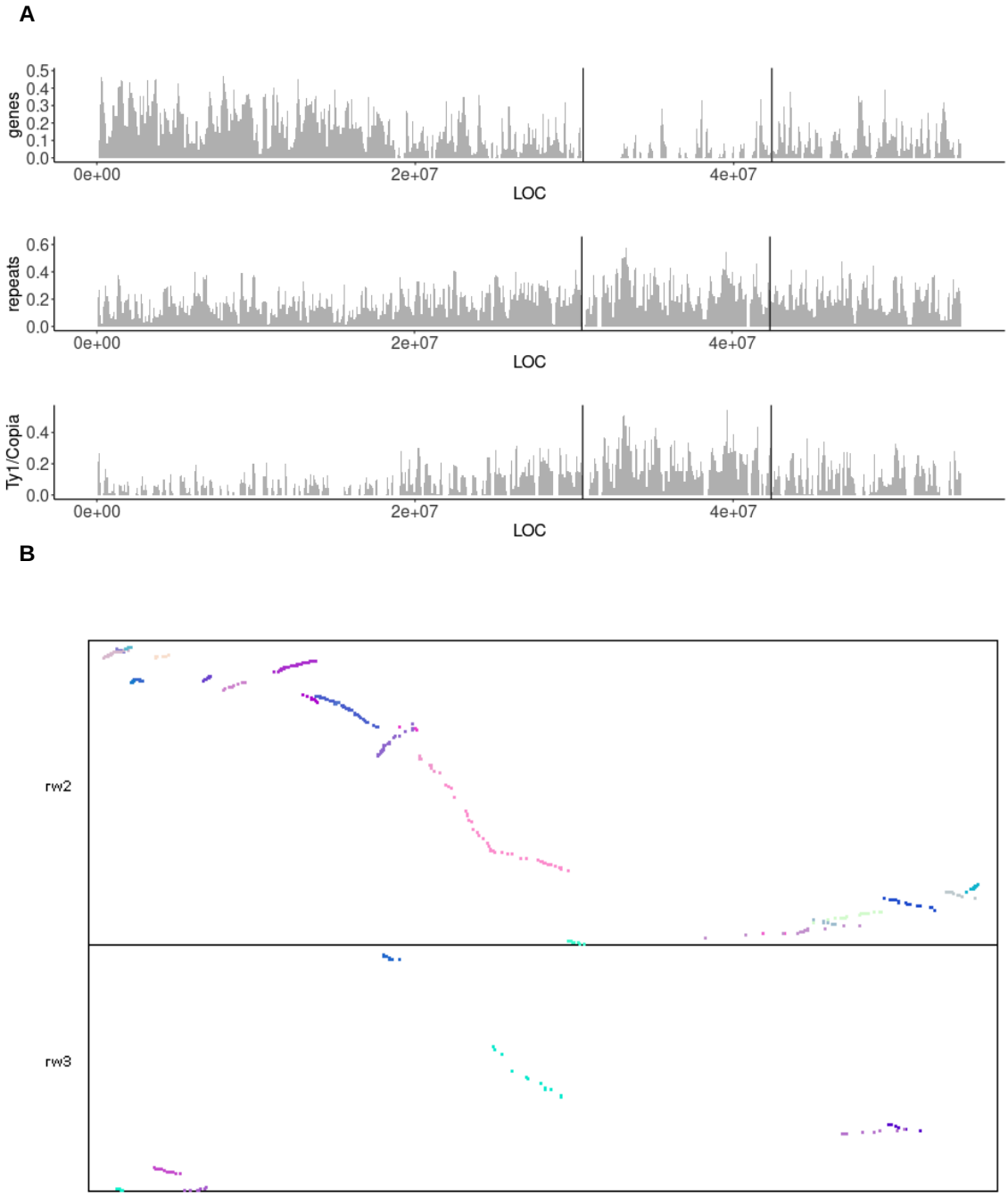

Supplementary Figure 10. Structure of cnv-chr4a. A) Gene density along chromosome 4, with lines denoting boundaries for cnv-chr4a. B) Repeat density along chromosome 4, with lines denoting boundaries for cnv-chr4a. C) Density of repeat family Ty1/Copia along chromosome 4, with lines denoting boundaries for cnv-chr4a. D) Syntenic relationships between chromosome 4 (x axis) with chromosomes 2 and 3. Colors are arbitrarily assigned denoting syntenic groups.

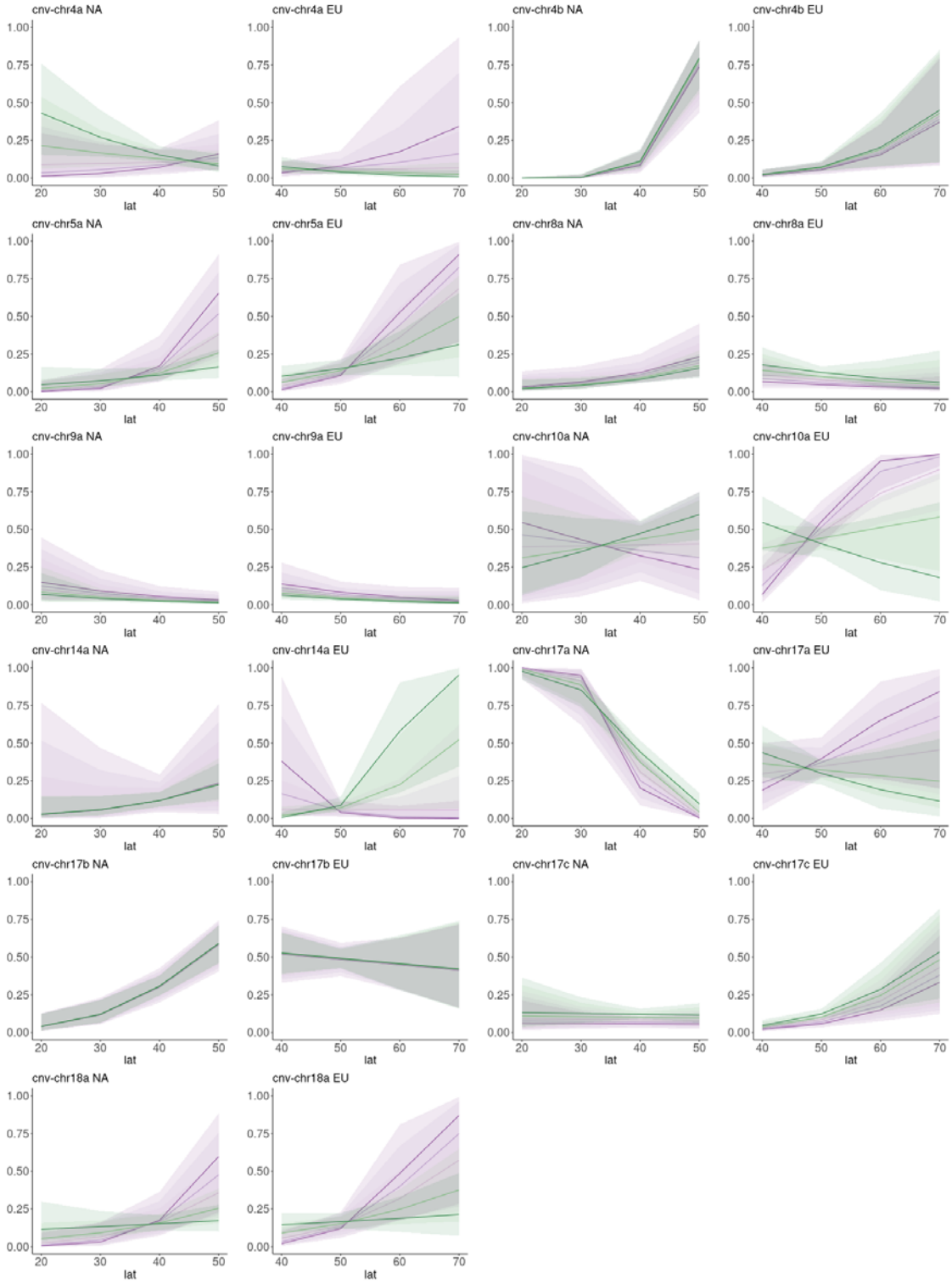

Supplementary Figure 11. Spatio-temporal CNV frequency shifts for 11 significant CNVrs for each range. Logistic regression models with error bands representing 95% CI of least-squares regressions of CNV frequency. Time binned into five categories, ranging from historic (purple) to modern (green). Model information found in Supplementary Table 6.